Inorg. Chem. **2005**, *44*, 6802–6827

Forum

Chemical Approaches to Artificial Photosynthesis. 2

James H. Alstrum-Acevedo, M. Kyle Brennaman, and Thomas J. Meyer*

Department of Chemistry, The University of North Carolina at Chapel Hill, CB #3290, Chapel Hill, North Carolina 27599-3290

Received June 3, 2005

The goal of artificial photosynthesis is to use the energy of the sun to make high-energy chemicals for energy production. One approach, described here, is to use light absorption and excited-state electron transfer to create oxidative and reductive equivalents for driving relevant fuel-forming half-reactions such as the oxidation of water to O_2 and its reduction to H_2. In this "integrated modular assembly" approach, separate components for light absorption, energy transfer, and long-range electron transfer by use of free-energy gradients are integrated with oxidative and reductive catalysts into single molecular assemblies or on separate electrodes in photelectrochemical cells. Derivatized porphyrins and metalloporphyrins and metal polypyridyl complexes have been most commonly used in these assemblies, with the latter the focus of the current account. The underlying physical principles—light absorption, energy transfer, radiative and nonradiative excited-state decay, electron transfer, proton-coupled electron transfer, and catalysis—are outlined with an eye toward their roles in molecular assemblies for energy conversion. Synthetic approaches based on sequential covalent bond formation, derivatization of preformed polymers, and stepwise polypeptide synthesis have been used to prepare molecular assemblies. A higher level hierarchial "assembly of assemblies" strategy is required for a working device, and progress has been made for metal polypyridyl complex assemblies based on sol–gels, electropolymerized thin films, and chemical adsorption to thin films of metal oxide nanoparticles.

I. Introduction

The goal of artificial photosynthesis is to mimic the green plants and other photosynthetic organisms that use sunlight to make high-energy chemicals.[1−8] This is a challenging goal because success requires integration of multiple chemical functions in a stable chemical architecture. As a result, artificial photosynthesis has developed more slowly than other approaches to solar energy conversion, namely, solid-state solar cells, interfacial TiO_2 photovoltaic cells, and organic thin film devices.[9−23]

(1) Meyer, T. J. *Acc. Chem. Res.* **1989**, *22*, 163.
(2) Gust, D.; Moore, T. A.; Moore, A. L. *Acc. Chem. Res.* **2001**, *34*, 40.
(3) Gust, D.; Moore, T. A. Intramolecular photoinduced electron-transfer reactions of porphyrins. In *The Porphyrin Handbook*; Gust, D., Moore, T. A., Eds.; Academic Press: New York, 1999; pp 153−190.
(4) Wasielewski, M. R. *Chem. Rev.* **1992**, *92*, 435.
(5) Balzani, V.; Moggi, L.; Scandola, F. Towards a supramolecular photochemistry: Assembly of molecular components to obtain photochemical molecular devices. In *Supramolecular Photochemistry*; Balzani, V., Moggi, L., Scandola, F., Eds.; D. Reidel: Dordrecht, The Netherlands, 1987; pp 1−28.
(6) Gust, D.; Moore, T. A.; Moore, A. L. *Acc. Chem. Res.* **1993**, *26*, 198.
(7) Arakawa, H.; Aresta, M.; Armor, J. N.; Barteau, M. A.; Beckman, E. J.; Bell, A. T.; Bercaw, J. E.; Creutz, C.; et al. *Chem. Rev.* **2001**, *101*, 953.
(8) Balzani, V.; Credi, A.; Venturi, M. Photoinduced charge separation and solar energy conversion. In *Molecular Devices and Machines: a Journey into the Nanoworld*; Balzani, V., Credi, A., Venturi, M., Eds.; Wiley-VCH: Weinheim, Germany, 2003; pp 132−173.
(9) Grätzel, M. *MRS Bull.* **2005**, *30*, 23.
(10) Grätzel, M. *J. Photochem. Photobiol. A* **2004**, *164*, 3.
(11) Grätzel, M. *Nature* **2001**, *414*, 338.
(12) Wang, P.; Dai, Q.; Zakeeruddin, S. M.; Forsyth, M.; MacFarlane, D. R.; Grätzel, M. *J. Am. Chem. Soc.* **2004**, *126*, 13590.
(13) Schmidt-Mende, L.; Bach, U.; Humphry-Baker, R.; Horiuchi, T.; Miura, H.; Ito, S.; Uchida, S.; Grätzel, M. *Adv. Mater.* **2005**, *17*, 813.
(14) Schmidt-Mende, L.; Zakeeruddin, S. M.; Grätzel, M. *Appl. Phys. Lett.* **2005**, *86*, 013504/1.
(15) Hara, K.; Sato, T.; Katoh, R.; Furube, A.; Yoshihara, T.; Murai, M.; Kurashige, M.; Ito, S.; Shinpo, A.; Suga, S.; Arakawa, H. *Adv. Funct. Mater.* **2005**, *15*, 246.
(16) Arakawa, H. *Taiyo Enerugi* **2005**, *31*, 11.
(17) Sayama, K.; Tsukagoshi, S.; Mori, T.; Hara, K.; Ohga, Y.; Shinpou, A.; Abe, Y.; Suga, S.; Arakawa, H. *Sol. Energy Mater. Sol. Cells* **2003**, *80*, 47.

10.1021/ic050904r CCC: $30.25
Published on Web 09/26/2005

The molecular complexity of the natural photosynthetic apparatus is both an object lesson that illustrates the difficulties involved and an inspiration to research in this area.[24−32] With successful application, artificial photosynthesis would shortcut the billions of years of evolution that led to working photosynthetic membranes. Using chemical design and the principles of chemistry and physics, its goals are simpler and far less demanding.

In natural photosynthesis in the higher green plants, a complex reaction scheme uses solar energy to convert H_2O into O_2 and reducing equivalents, which appear as NADPH. In photosystem I, the reducing equivalents in NADPH are used to reduce CO_2 to carbohydrates, eq 1, or in bacteria, used directly as a reductive energy source.[25−32] In artificial photosynthesis, the goal is to harness the energy of the sun to drive high-energy small-molecule reactions such as water splitting, eq 2, or CO_2 reduction, eq 3.

$$6H_2O + 6CO_2 + 48h\nu \rightarrow C_6H_{12}O_6 + 6O_2 \quad (1)$$

$$2H_2O + 4h\nu \rightarrow 2H_2 + O_2 \quad (2)$$

$$2H_2O + 2CO_2 + 4h\nu \rightarrow 2HCOOH + O_2 \quad (3)$$

The high-energy chemicals that form in these reactions can be recombined to extract the stored chemical energy. An ultimate goal is water splitting with the photochemically produced hydrogen and oxygen recombined in high-efficiency fuel cells for electricity production (Scheme 1).

Other small-molecule reactions are potential targets, and applications may exist in "green chemistry" for making high-value-added chemicals. For example, a high-efficiency photoelectrochemical synthesis (PES) cell has been reported for the production of Br_2 and H_2O_2.[33]

Scheme 1. Photochemical Water Splitting Coupled to a Hydrogen/Oxygen Fuel Cell

Photochemical: $2H_2O + 4h\nu \rightarrow 2H_2 + O_2$

Fuel Cell: $2H_2 \rightarrow 4H^+ + 4e^-$ (anode)

$O_2 + 4\,H^+ + 4\,e^- \rightarrow 2H_2O$ (cathode)

$2H_2 + O_2 \rightarrow 2H_2O$: $\Delta G^o = -4.92$ eV (−113 kcal/mol)

The energy-storage reactions in eqs 1−3 are all oxidation−reduction (redox) reactions and can be divided into half-reactions. Each half-reaction involves a multiple electron change. This and the high-energy content of intervening $1e^-$ intermediates such as $CO_2^{\bullet-}$ or $^{\bullet}OH$ ensure that both the photochemical fuel-forming reactions and their subsequent recombination are slow under ambient conditions. Both half-reactions must be catalyzed if they are to occur at appreciable rates at or near room temperature.

Resolution into half-reactions provides the basis for a "modular" approach to artificial photosynthesis. As in natural photosynthesis, separate half-reactions can be addressed separately and combined at a later stage into a single device. Complexity is unavoidable because of multifunctional requirements (light absorption, energy transfer, electron transfer, redox catalysis). There is a need to arrange and integrate functional groups and to provide an overall structural hierarchy.

A system analysis leads to the concept of the "integrated modular assembly" as described in an *Accounts of Chemical Research* article in 1989[1] and more recently in an article in *Coordination Chemistry Reviews*.[34] The current account is a "do it yourself" guide to constructing working assemblies for artificial photosynthesis.

Two approaches have dominated research in this area. One has been based on porphyrins and metalloporphyrins as chromophores and their incorporation into molecular assemblies.[2,3,6] A second is based on the metal-to-ligand charge-transfer (MLCT) excited states of metal polypyridyl complexes. Both approaches utilize the same underlying physical principles, and both utilize systematic molecular assembly strategies.

II. Integrated Approach to Artificial Photosynthesis Based on Polypyridyl Complexes. Functional Elements

II.A. Spatially Integrated Molecular Assemblies. In the integrated modular approach, reaction "modules" are linked together to construct reactive molecular assemblies. Energy conversion is based on light absorption and electron transfer. There is an analogy with natural photosynthesis where both CO_2 reduction in photosytem I and water oxidation in photosystem II are triggered by light absorption and excited-state electron transfer in the *reaction centers* of photosynthetic membranes.[24,30,35−41]

(18) Hara, K.; Kurashige, M.; Dan-oh, Y.; Kasada, C.; Shinpo, A.; Suga, S.; Sayama, K.; Arakawa, H. *New J. Chem.* **2003**, *27*, 783.
(19) Hara, K.; Kurashige, M.; Ito, S.; Shinpo, A.; Suga, S.; Sayama, K.; Arakawa, H. *Chem. Commun.* **2003**, *2*, 252.
(20) Hara, K.; Sato, T.; Katoh, R.; Furube, A.; Ohga, Y.; Shinpo, A.; Suga, S.; Sayama, K.; Sugihara, H.; Arakawa, H. *J. Phys. Chem. B* **2003**, *107*, 597.
(21) Kalyanasundaram, K.; Grätzel, M. *Coord. Chem. Rev.* **1998**, *177*, 347−414.
(22) Nozik, A. J. *Annu. Rev. Phys. Chem.* **2001**, *52*, 193.
(23) Adams, D. M.; Brus, L.; Chidsey, C. E. D.; Creager, S.; Creutz, C.; Kagan, C. R.; Kamat, P. V.; Lieberman, M.; Lindsay, S.; Marcus, R. A.; Metzger, R. M.; Michel-Beyerle, M. E.; Miller, J. R.; Newton, M. D.; Rolison, D. R.; Sankey, O.; Schanze, K. S.; Yardley, J.; Zhu, X. *J. Phys. Chem. B* **2003**, *107*, 6668.
(24) Ferreira, K. N.; Iverson, T. M.; Maghlaoui, K.; Barber, J.; Iwata, S. *Science* **2004**, *303*, 1831.
(25) Jordan, P.; Fromme, P.; Witt, H. T.; Klukas, O.; Saenger, W.; Krauss, N. *Nature* **2001**, *411*, 909.
(26) Blankenship, R. E. *Molecular Mechanisms of Photosynthesis*; Blackwell Science: Oxford, U.K., 2002.
(27) Britt, R. D. In *Oxygenic Photosynthesis: The Light Reactions*; Britt, R. D., Ed.; Kluwer Academic Publishers: Dordrecht, The Netherlands, 1996; pp 137−164.
(28) Renger, G. *Biochim. Biophys. Acta* **1992**, *1503*, 210.
(29) *Molecular Bioenergetics: Simulations of Electron, Proton, and Energy Transfer*; American Chemical Society: Washington, DC, 2004.
(30) Jungas, C.; Ranck, J.-L.; Rigaud, J.-L.; Joliot, P.; Vermeglio, A. *EMBO J.* **1999**, *18*, 534.
(31) Danks, S. M.; Evans, E. H.; Whittaker, P. A. *Photosynthetic Systems: Structure, Function, and Assmebly*; John Wiley and Sons: New York, 1985.
(32) Lawlor, D. W. *Photosynthesis*; Springer-Verlag: New York, 2001.
(33) Otruba, J. P.; Neyhart, G. A.; Dressick, W. J.; Marshall, J. L.; Sullivan, B. P.; Watkins, P. A.; Meyer, T. J. *J. Photochem.* **1986**, *35*, 133.
(34) Huynh, M. H. V.; Dattelbaum, D. M.; Meyer, T. J. *Coord. Chem. Rev.* **2005**, *249*, 457.
(35) Barber, J. *Q. Rev. Biophys.* **2003**, *36*, 71.
(36) Diner, B. A.; Babcock, G. T. Structure, dynamics, and energy conversion efficiency in photosystem II. In *Advances in Photosynthesis: The Light Reactions*; Diner, B. A., Babcock, G. T., Eds.; Kluwer Academic Publishers: Dordrecht, The Netherlands, 1996; Vol. 4, pp 213−247.

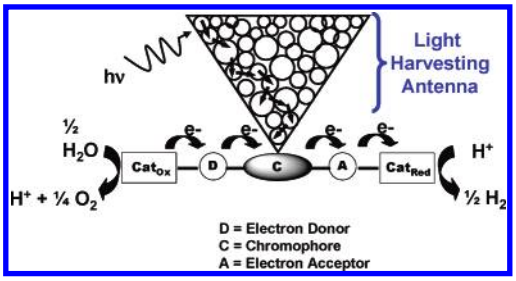

Figure 1. Diagram illustrating the essential elements in an assembly for artificial photosynthesis and the sequence of events that occurs after light is absorbed. The abbreviations are C = chromophore (light absorber), D = electron transfer donor, A = electron-transfer acceptor, cat_{red} = catalyst for chemical reduction, and cat_{ox} = catalyst for chemical oxidation. The reaction illustrated is the photochemical splitting of water into H_2 and O_2. In the absence of a light-harvesting array, multilayer structures are required to achieve sufficient light absorption.

Figure 1 illustrates what may be the minimum number of elements and processes required in a molecular assembly for artificial photosynthesis:

(1) *Light absorption*, either at a single "reaction center" chromophore (C) or by excitation of an antenna array, followed by energy-transfer sensitization of C*. Single-molecule light absorption is low, requiring the use of antenna arrays or multilayer structures for efficient light harvesting. The absorbance (Abs) of a surface layer of chromophore of coverage Γ (in mol/cm^2) and molar extinction coefficient ϵ (in M^{-1} cm^{-1}) is given by Abs $= 10^3\epsilon\Gamma$. Even with $\epsilon =$ 10 000, Abs $= 10^{-3}$ for a monolayer coverage of 10^{-10} mol/cm^2. Absorption of 90% of the light requires Abs $= 1$.

(2) *Electron-transfer quenching*, of a donor−chromophore−acceptor (D−C−A) array either oxidatively, D−C*−A → D−C$^+$−A$^-$, or reductively, D−C*−A → D$^+$−C$^-$−A. The driving force for either is a favorable free-energy change with $\Delta G° < 0$.

(3) *Redox separation by electron transfer*, D−C$^+$−A$^-$ → D$^+$−C−A$^-$ or D$^+$−C$^-$−A → D$^+$−C−A$^-$, also driven by $\Delta G° < 0$. The combination of processes in (2) and (3) uses free-energy gradients to give spatially separated oxidative and reductive redox equivalents stored as D$^+$ and A$^-$. This is analogous to a p/n junction in a Si semiconductor, which separates photochemically produced electron−hole pairs.[42−47]

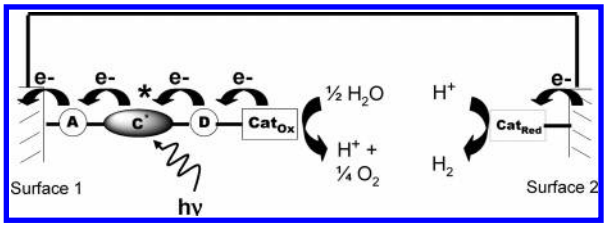

Figure 2. Schematic diagram for an integrated, modular PES cell for water splitting illustrating photoinduced electron transfer from catalyst cat_{ox} to catalyst cat_{red}.

(4) *Electron-transfer activation of catalysts*, from A$^-$ to a catalyst for reduction, cat_{red}, and to D$^+$ from a second catalyst, cat_{ox}, for oxidation. The potentials of the $D^{+/0}$ and $A^{0/-}$ couples dictate $E°'$ for the individual fuel-forming half-reactions and the overall free-energy change, $\Delta G°$. $\Delta G°$ cannot exceed the free-energy content of the excited state above the ground state, $\Delta G_{ET}°$, with $\Delta G°$ (eV) $= -F[E°(D^{+/0}) - E°(A^{0/-})] \leq \Delta G_{ET}°$ (eV). F is the Faraday constant, 96 485 C/mol of electrons or 1 eV/V in SI units.

(5) *Multiple electron transfer* and repetition of the light absorption−electron-transfer sequence to give the required number of reductive or oxidative equivalents at cat_{ox} and cat_{red} to carry out the half-reactions. For CO_2 reduction to HCOOH, $n = 2$, and for water oxidation to O_2, $n = 4$.

(6) *Reaction of the activated catalysts*, with H_2O, H^+, CO_2, etc., to give the final energy conversion products returning the catalysts to the cat_{ox} and cat_{red} states, ending a catalytic cycle.

II.B. Photoelectrochemistry. Photoelectrochemical Synthesis (PES) Cells. Another approach, utilized in PES cells, is to carry out the half-reactions at the separate electrodes of an electrochemical cell. The potential required to drive the reaction is provided by light rather than by a battery or some other applied energy source.

This simplifies integration. The half-reactions are connected by electron transfer through an external circuit with ion flow between cell compartments to maintain charge neutrality. It does require stable interfacial links to attached molecules and molecular assemblies. These links must also support facile electron transfer to and from electrode or semiconductor surfaces.

In a PES cell, the electrode(s) can function in two ways.

(i) Electrode as an Electroactive Interface. In one approach, the electrode acts only as a conductive interface for transferring electrons between catalyst assemblies at separate electrodes. This is schematically illustrated in Figure 2. In Figure 2, light absorption and electron transfer occur initially to give (surface 1)−A$^-$−C−D−$(cat_{ox})^+$. This is followed by interfacial and interelectrode electron transfer to give (surface 2)−$(cat_{red})^-$. Repetition would build up multiple redox equivalents and initiate the half-reactions.

As diagrammed in Figure 2, the PES cell for water splitting would also produce a photopotential and photocurrent driven by the potential difference between the surface $A^{0/-}$ and $cat_{red}^{0/-}$ couples. More complex surface structures such as

(37) (a) Diner, B. A.; Rappaport, F. *Annu. Rev. Plant Biol.* **2002**, *53*, 551. (b) Grotjohann, I.; Jolley, C.; Fromme, P. *Phys. Chem. Chem. Phys.* **2004**, *6*, 4743.
(38) Hu, X.; Damjanovic, A.; Ritz, T.; Schulten, K. *Proc. Natl. Acad. Sci. U.S.A.* **1998**, *95*, 5935.
(39) Cogdell, R. J.; Gardiner, A. T.; Roszak, A. W.; Law, C. J.; Southall, J.; Isaacs, N. W. *Photosynth. Res.* **2004**, *81*, 207.
(40) Li, Y.-F.; Zhou, W.; Blankenship, R. E.; Allen, J. P. *J. Mol. Biol.* **1997**, *271*, 456.
(41) Webber, A. N.; Lubitz, W. *Biochim. Biophys. Acta* **2001**, *1507*, 61.
(42) Carabe, J.; Gandia, J. J. *Opt. Electron. Rev.* **2004**, *12*, 1.
(43) Tobias, I.; Del Canizo, C.; Alonso, J. Crystalline silicon solar cells and modules. In *Handbook of Photovoltaic Science and Engineering*; Tobias, I., Del Canizo, C., Alonso, J., Eds.; John Wiley & Sons Ltd.: Chichester, U.K., 2003.
(44) Schropp, R. E. I. *Thin Solid Films* **2004**, *451−452*, 455.
(45) Shah, A. V.; Meier, J.; Vallat-Sauvain, E.; Wyrsch, N.; Kroll, U.; Droz, C.; Graf, U. *Sol. Energy Mater. Sol. Cells* **2003**, *78*, 469.
(46) Zeman, M. New trends in thin-film silicon solar cell technology. In *Proceedings of the International Conference on Advanced Semiconductor Devices and Microsystems*; Zeman, M., Ed.; Institute of Electrical and Electronics Engineers: New York, 2002.
(47) Torchynska, T. V.; Polupan, G. P. *Semicond. Phys., Quantum Electron. Optoelectron.* **2002**, *5*, 63.

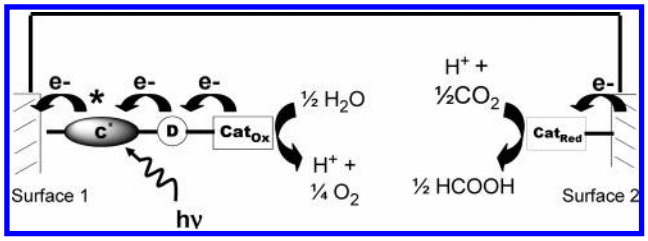

Figure 3. Schematic diagram illustrating the photoelectrochemical reaction between CO and H_2O to give HCOOH and O_2 initiated by excitation and photoinjection from an adsorbed chromophore to the conduction band of TiO_2.

(surface 1)−A−C−C−C−C−C−cat_{ox} could help meet the requirement for multiple molecular light absorption but only if efficient, random-walk C* → C energy transfer occurs to the quencher where electron transfer occurs.[34,48]

Appropriate, transparent, high-surface-area electrodes are known for such applications, for example, nanoparticle thin films of doped SnO_2.[49] There is also an extensive photochemistry of surface-adsorbed, monolayer D−C−A molecular assemblies on Au surfaces.[50]

(ii) Electrode as an Active Modular Component. The electrode itself can be an active element. An example, pioneered by Grätzel and co-workers, is photoinjection into TiO_2 by the excited states of adsorbed chromophores including polypyridyl complexes of Ru^{II} such as *cis*-Ru(4,4′-$(COOH)_2$bpy)$_2$$(NCS)_2$.[9,10,51,52] The carboxylic acid groups bind by the formation of surface ester bonds and by H bonding.

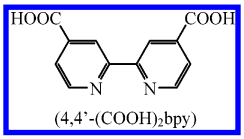

In a Grätzel cell, which utilizes a mesoporous, high-surface-area TiO_2 film, excitation and quenching occur by electron transfer to the conduction band of the semiconductor, TiO_2−Ru^{II} + hν → TiO_2−Ru^{II*} → $^-TiO_2$−Ru^{III}. Surface Ru^{III} is subsequently reduced by I^-, $2TiO_2$−Ru^{III}, $3I^-$ → $2TiO_2$−Ru^{II}, I_3^-. The cell is completed by I_3^- reduction at an inert cathode, $2e^-$(cathode) + I_3^- → cathode + $3I^-$. This sequence provides the chemical basis for a photovoltaic device with a maximum photopotential arising from the potential difference between the Fermi level in the conduction band and $E^{\circ\prime}$ for the I_3^-/I^- couple.

Photoinjection and surface reduction of Ru^{III} are complete on the nanosecond time scale. Back electron transfer from the bulk of the semiconductor to adsorbed Ru^{III} is far slower. This and the small transit volumes for conduction-band electrons to the underlying electrode result in efficient collection of the photoproduced electrons.

Possible application of this approach to artificial photosynthesis and the fuel-forming reaction in eq 3 is illustrated in Figure 3, which highlights the electrode as the initial electron acceptor rather than a molecular unit in a molecular assembly.

The modular approach in Figure 3 is general including possible applications in "green chemistry". Reactions such as olefin epoxidation by water, eq 4, or dehydrogenation of alcohols, eq 5, could be accessible by varying the catalyst linked to the phtotoanode.

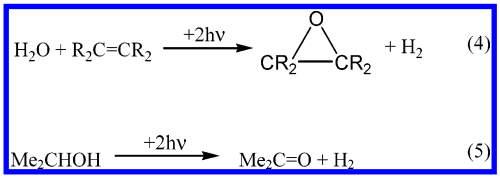

Such cells would produce a photocurrent at a maximum photopotential equal to the potential difference between the Fermi level of the TiO_2 conduction band and $E^{\circ\prime}$ for the $cat_{red}^{-/0}$ couple. Photochemical dehydrogenation of 2-propanol in eq 5 has been demonstrated for [(4,4′-$(CO_2H)_2$bpy)-(4,4′-Me_2bpy)Ru_a^{II}(dpp)Ru_b^{II}(tpy)(OH_2)]$^{4+}$ adsorbed on TiO_2, although with low efficiency (section 7.3, ref 53).

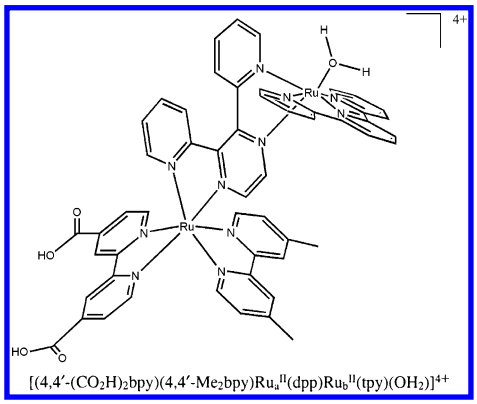

III. Modules. Light Absorption and Excited States

III.A. Introduction. (i) Excited-State Redox Potentials. Quenching and flash photolysis measurements were used in the early 1970s to demonstrate excited-state electron transfer. Early work focused on MLCT excited states of $[Ru(bpy)_3]^{2+}$ (bpy is 2,2′-bipyridine) and its derivatives and the $\pi-\pi^*$ excited states of porphyrins.[54−56]

$[Ru(bpy)_3]^{2+}$ absorbs light in the visible region with λ_{max} = 452 nm in CH_3CN (ϵ = 13 000 M^{-1} cm^{-1}). MLCT excitation, $^1(d\pi^6)$ → $^1(d\pi^5\pi^*)$, is followed by rapid (τ < 1 ps) relaxation to the lowest triplet state, $[Ru(bpy)_3]^{2+}$*, ^{3}-($d\pi^5\pi^*$). The lowest "triplet" is split by low symmetry and

(48) Fleming, C. N.; Jang, P.; Meyer, T. J.; Papanikolas, J. M. *J. Phys. Chem. B* **2004**, *108*, 2205.
(49) Nutz, T.; Felde, U.; Haase, M. *J. Chem. Phys.* **1999**, *110*, 12142.
(50) Ma, H.; Jen, K.-Y. *Spectrum* **2004**, *17*, 24−29 and references cited therein.
(51) Nazeeruddin, M. K.; Kay, A.; Rodicio, I.; Humphry-Baker, R.; Mueller, E.; Liska, P.; Vlachopoulos, N.; Grätzel, M. *J. Am. Chem. Soc.* **1993**, *115*, 6382.
(52) Benko, G.; Kallioinen, J.; Korppi-Tommola, J. E. I.; Yartsev, A. P.; Sundstrom, V. *J. Am. Chem. Soc.* **2002**, *124*, 489.
(53) Treadway, J. A.; Moss, J. A.; Meyer, T. J. *Inorg. Chem.* **1999**, *38*, 4386.
(54) Balzani, V.; Bolleta, F.; Gandolfi, M. T.; Maestri, M. *Top. Curr. Chem.* **1978**, *75*, 1.
(55) Sutin, N.; Creutz, C. *Pure Appl. Chem.* **1980**, *52*, 2717
(56) Meyer T. J. *Progress in Inorganic Chemistry*; Wiley & Sons: New York, 1983; pp 389−440 and references cited therein.

Scheme 2. Excited- and Ground-State Redox Potentials (vs SCE in CH_3CN) for $[Ru(bpy)_3]^{2+}$ in CH_3CN at 25 °C[a]

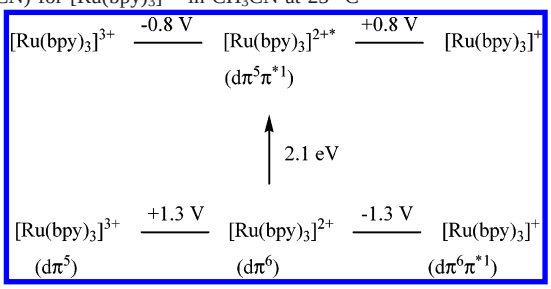

[a] The potentials are related by $E°(ES^{+/0}) = E_o(GS^{+/0}) - \Delta G_{ES}°/F$ and $E°(ES^{0/-}) = E°(GS^{0/-}) + \Delta G_{ES}°/F$ with F the Faraday (1 eV/V).[54−56]

spin−orbit coupling into three low-lying states separated by ~30 cm^{-1}. Because of spin−orbit coupling in the $d\pi^5$ core, low-lying triplet excited states are mixed with higher-lying singlet excited states. The lifetime of $[Ru(bpy)_3]^{2+}*$ is ~1 μs, depending on the medium and temperature.[57−59]

$[Ru(bpy)_3]^{2+}*$ undergoes facile electron transfer. The impact of excited-state formation on redox potentials is illustrated in Scheme 2. These data show that the oxidizing and reducing abilities of $[Ru(bpy)_3]^{2+}$ are enhanced in $[Ru(bpy)_3]^{2+}*$ by $\Delta G_{ES}° = 2.1$ eV, the free-energy content of the excited state above the ground state. Ground-state ($GS^{+/0}$/$GS^{0/-}$) and excited-state redox potentials ($ES^{+/0}$/$ES^{0/-}$) are related by $E°(ES^{+/0}) = E°(GS^{+/0}) - \Delta G_{ES}°/F$ and $E°(ES^{0/-}) = E°(GS^{0/-}) + \Delta G_{ES}°/F$.[54−56]

At pH = 8, $[Ru(bpy)_3]^{2+}*$ is thermodynamically capable of oxidizing water ($E°(pH = 8) = -0.76$ V) and reducing CO_2 ($E° = -0.67$ V). The full excited-state energy can be utilized by initial oxidative quenching

$$[Ru(bpy)_3]^{2+}* \rightarrow [Ru(bpy)_3]^{3+} + e^- \qquad (E° = -0.8\ V)$$

followed by reduction of $[Ru(bpy)_3]^{3+}$

$$[Ru(bpy)_3]^{3+} + e^- \rightarrow [Ru(bpy)_3]^{2+} \qquad (E° = 1.3\ V)$$

or by reductive quenching followed by oxidation of $[Ru(bpy)_3]^{+}$

$$[Ru(bpy)_3]^{2+}* + e^- \rightarrow [Ru(bpy)_3]^{+} + e^- \qquad (E° = 0.8\ V)$$

$$[Ru(bpy)_3]^{+} \rightarrow [Ru(bpy)_3]^{2+} + e^- \qquad (E° = -1.3\ V)$$

(ii) Molecular Assemblies for Directed (Vectorial) Excited-State Electron Transfer. Excited-state electron transfer was demonstrated by flash photolysis experiments in solutions containing $[Ru(bpy)_3]^{2+}$ in the presence of electron-transfer donors, such as 10-methylphenothiazine (10-MePTZ), or acceptors, such as methylviologen (MV^{2+}) (Scheme 3).[56,60−64]

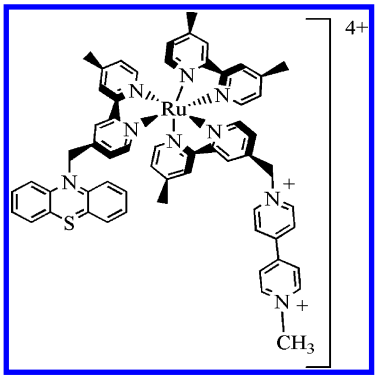

Figure 4. Early donor−chromophore−acceptor assembly.[74,75]

Scheme 3. Reaction Scheme Illustrating Energy Conversion Based on Excited-State Electron-Transfer Quenching

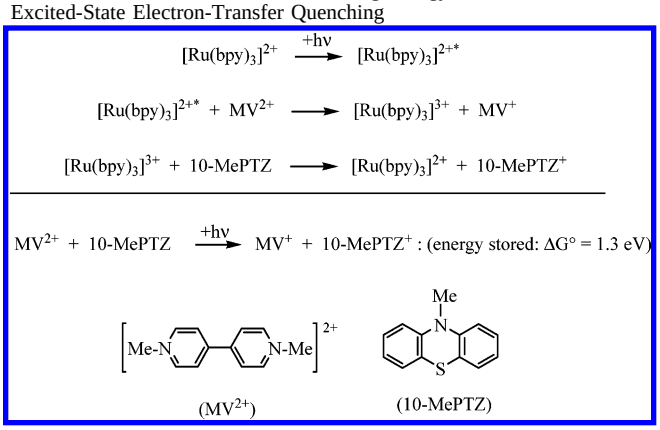

The reaction in Scheme 3 provided an early conceptual basis for artificial photosynthesis. Visible light was used to drive an endoergic chemical reaction, $\Delta G° = +1.3$ eV, in which neither of the reactants absorb visible light.[64]

The next step was to combine these functions in D−C−A assemblies in which oxidative and reductive equivalents are created and separated by free-energy gradients.[1−3,34,58,59,65−73] An early example based on polypyridyl complexes is shown in Figure 4. Excitation of the Ru(bpy) MLCT chromophore and electron transfer led to $(PTZ^{\bullet+})Ru^{II}(MV^{\bullet+})$, with the transiently stored redox equivalents as $PTZ^{\bullet+}$ and $MV^{\bullet+}$ spatially separated in a single molecule.[74,75]

Application of transient laser techniques, first on the nanosecond and then picosecond time scales, with absorption

(57) Meyer, T. J. *Pure Appl. Chem.* **1986**, *58*, 1193.
(58) Hicks, C.; Ye, G.; Levi, C.; Gonzales, M.; Rutenburg, I.; Fan, J.; Helmy, R.; Kassis, A.; Gafney, H. D. *Coord. Chem. Rev.* **2001**, *211*, 207.
(59) Shan, B.-Z.; Zhao, Q.; Goswami, N.; Eichhorn, D. M.; Rillema, D. P. *Coord. Chem. Rev.* **2001**, *211*, 117.
(60) Bock, C. R.; Meyer, T. J.; Whitten, D. G. *J. Am. Chem. Soc.* **1974**, *96*, 4710.
(61) Demas, J. N.; Adamson, A. W. *J. Am. Chem. Soc.* **1973**, *95*, 5159.
(62) Adamson, A. W.; Demas, J. N. *J. Am. Chem. Soc.* **1971**, *93*, 1800.
(63) Gafney, H.; Adamson, A. W. *J. Am. Chem. Soc.* **1972**, *94*, 8238.
(64) Young, R. C.; Meyer, T. J.; Whitten, D. G. *J. Am. Chem. Soc.* **1976**, *98*, 286.
(65) Meyer, T. J. *Intramolecular control of light induced electron transfer*; Reidel Publishing Co.: Dordrecht, Holland, 1987; Vol. 214, pp 103−120.
(66) Meyer, T. J. *Pure Appl. Chem.* **1990**, *62*, 1003.
(67) Sullivan, B. P.; Abruna, H.; Finklea, H. O.; Salmon, D. J.; Nagle, J. K.; Meyer, T. J.; Sprintschnik, H. *Chem. Phys. Lett.* **1978**, *58*, 389.
(68) Westmoreland, T. D.; Schanze, K. S.; Neveux, P. E., Jr.; Danielson, E.; Sullivan, B. P.; Chen, P.; Meyer, T. J. *Inorg. Chem.* **1985**, *24*, 2596.
(69) Balzani, V.; Juris, A. *Coord. Chem. Rev.* **2001**, *211*, 97.
(70) Kalyanasundaram, K. *Photochemistry in Microheterogeneous Systems*; Academic: Orlando, FL, 1987.
(71) Lee, W.-Y. *Mikrochim. Acta* **1997**, *127*, 19.
(72) Schanze, K. S.; MacQueen, D. B.; Perkins, T. A.; Cabana, L. A. *Coord. Chem. Rev.* **1993**, *122*, 63.
(73) Balzani, V.; Credi, A.; Venturi, M. *Molecular Devices and Machines—A Journey into the Nano World*; Wiley-VCH: Weinheim, Germany, 2004.
(74) Danielson, E.; Elliott, C. M.; Merkert, J. W.; Meyer, T. J. *J. Am. Chem. Soc.* **1987**, *109*, 2519.

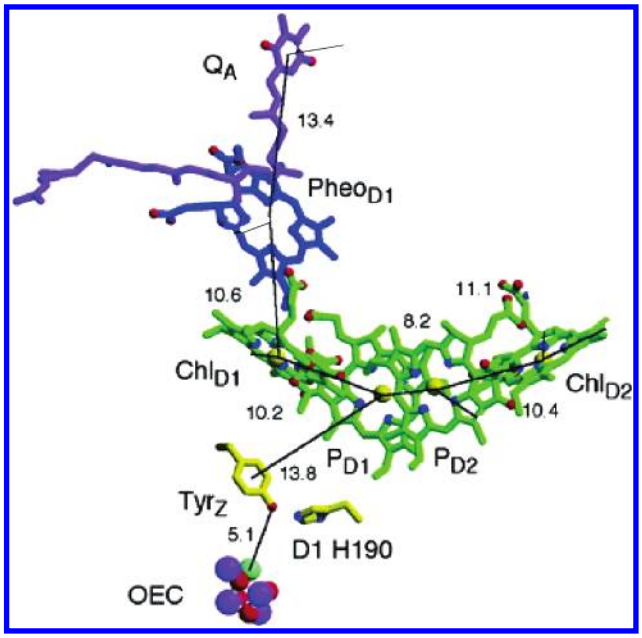

Figure 5. Molecular structure of the reaction center of photosystem II illustrating the $Tyr_Z-Chl_{D1}-Pheo_{D1}-Q_A$ donor−chromophore−acceptor (D−C−A−A′) array. Reprinted with permission from ref 24. Copyright 2004 American Association for the Advancement of Science.

monitoring provided the key evidence for photochemical electron transfer in these assemblies. By using these techniques, it was possible to observe the loss of characteristic absorption features for the excited state and characteristic growth in absorbances for $PTZ^{\bullet+}$ at 480 nm and $MV^{\bullet+}$ at 605 nm. These measurements also allowed the rate constants for the following $MV^+ \rightarrow PTZ^{\bullet+}$ back-electron-transfer reaction to be measured.

The D−C−A assembly in the photosystem II reaction center from a recent 3.5-Å-resolution crystal structure is shown in Figure 5.[24] Excitation of chlorophyll P_{680}, Chl_{D1} in Figure 5, is followed by electron transfer through pheophytin $Pheo_{D1}$ to the quinone acceptor, Q_A. Subsequent reduction of P_{680}^+ occurs by electron transfer from tyrosine Tyr_Z, which is H-bonded to histidine-190 (His-190).

III.B. Light Absorption and Energy-Transfer Sensitization. (i) Absorption. Light absorption or antenna and energy-transfer sensitization initiate the electron-transfer sequences in Figures 1 and 2. The peak intensity in the solar spectrum appears in the visible just below 500 nm, and the spectrum extends well into the near-IR. In a single-junction photovoltaic cell, an ideal sensitizer would convert sunlight to electricity below a threshold wavelength of 920 nm.[10] The energy at this wavelength, 10 870 cm^{-1} (1.35 eV), approaches a minimum threshold for the energy required for a useful fuel-forming reaction.

Single-molecule absorption is low, and spectral envelopes are typically relatively narrow.[76−79] In the spectrum of $[Ru(bpy)_3]^{2+}$ in Figure 6, the bands at 452 and ∼320 nm arise from $^1(d\pi^6) \rightarrow {}^1(d\pi^5\pi^{*1})$ MLCT transitions to the first and second π^*-acceptor levels on bpy. The intense band at 292 nm arises from a bpy-based $\pi \rightarrow \pi^*$ transition. Because there are three bpy ligands and three $d\pi$ orbitals, the detailed electronic structure is complex, giving rise to a series of closely spaced, overlapping MLCT bands.[78,80−89]

The intense, broad MLCT absorption band for $[Ru(bpy)_3]^{2+}$ at $\lambda_{max} = 452$ nm in CH_3CN has a bandwidth at half-maximum, $\Delta\bar{\nu}_{1/2}$, of ∼3600 cm^{-1}. The spectral width of the visible and onset of the near-IR from 400 to 900 nm is 13 900 cm^{-1}. To span this entire spectral region with high absorptivity requires either multiple absorptions in a single chromophore or an antenna apparatus containing chromophores that absorb in different spectral regions.

An example of the former strategy for MLCT absorbers is illustrated in Figure 6. In this strategy, multiple acceptor polypyridyl ligands with different π^*-acceptor levels were used to broaden light absorption over an extended spectral range. The dithiocarbamate anion ligand (dtc^-) was added to shift the MLCT bands to lower energy. This moves higher energy $d\pi \rightarrow \pi_2^*$ MLCT bands from the UV into the high-energy visible, further broadening the visible spectrum. The combined effect makes $[Ru((4,4'\text{-}COOEt)_2bpy)(dpb)(dtc)]^+$ a "black absorber", which absorbs light broadly throughout the visible into the near-IR.[80,90,91]

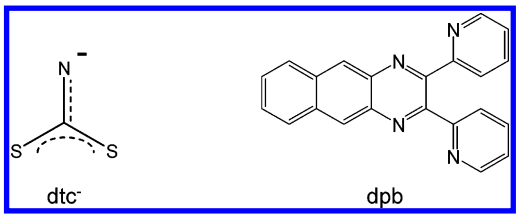

Band Shapes and Intensities. For a Gaussian-shaped band in the classical limit, the energy maximum, E_{abs}, and bandwidth at half-height, $\Delta\bar{\nu}_{1/2}$, are given in eqs 6 and 7 in the limit that $h\nu = h\nu'$ with no frequency changes for the coupled vibrations and solvent.

$$E_{abs} = \Delta G^\circ + \lambda \tag{6}$$

$$(\Delta\bar{\nu}_{1/2})^2 = 16\lambda k_B T \ln 2 \tag{7}$$

(75) Treadway, J. A.; Rutherford, T. J.; Chen, P.-Y.; Keene, F. R.; Meyer, T. J. *J. Phys. Chem. A* **1997**, *101*, 6824.
(76) Marcus, R. A. *J. Phys. Chem.* **1989**, *93*, 3078.
(77) Mataga, N.; Kubota, T. *Molecular Interactions and Electronic Spectra*; Dekker: New York, 1970; Chapter 3, p 107.
(78) Kober, E. M.; Meyer, T. J. *Inorg. Chem.* **1984**, *23*, 3877.
(79) Steinfeld, J. I. *An Introduction to Modern Molecular Spectroscopy*; The MIT Press: Cambridge, MA, 1985.
(80) Anderson, P. A.; Keene, F. R.; Meyer, T. J.; Moss, J. A.; Strouse, G. F.; Treadway, J. A. *J. Chem. Soc., Dalton Trans.* **2002**, *20*, 3820.
(81) Kober, E. M.; Meyer, T. J. *Inorg. Chem.* **1982**, *21*, 3967.
(82) Kober, E. M.; Meyer, T. J. *Inorg. Chem.* **1983**, *22*, 1614.
(83) Thompson, D. G.; Schoonover, J. R.; Timpson, C. J.; Meyer, T. J. *J. Phys. Chem. A* **2003**, *107*, 10250.
(84) Yersin, H.; Humbs, W.; Strasser, J. *Coord. Chem. Rev.* **1997**, *159*, 325.
(85) Braun, D.; Huber, P.; Wudy, J.; Schmidt, J.; Yersin, H. *J. Phys. Chem.* **1994**, *98*, 8044.
(86) Yersin, H.; Schuetzenmeier, S.; Wiedenhofer, H.; von Zelewsky, A. *J. Phys. Chem.* **1993**, *97*, 16496.
(87) Braun, D.; Hensler, G.; Gallhuber, E.; Yersin, H. *J. Phys. Chem.* **1991**, *95*, 1067.
(88) Riesen, H.; Wallace, L.; Krausz, E. J. *J. Chem. Phys.* **1995**, *102*, 4823.
(89) Riesen, H.; Wallace, L.; Krausz, E. J. *Int. Rev. Phys. Chem.* **1997**, *16*, 291.
(90) Strouse, G. F.; Anderson, P. A.; Schoonover, J. R.; Meyer, T. J.; Keene, F. R. *Inorg. Chem.* **1992**, *31*, 3004.

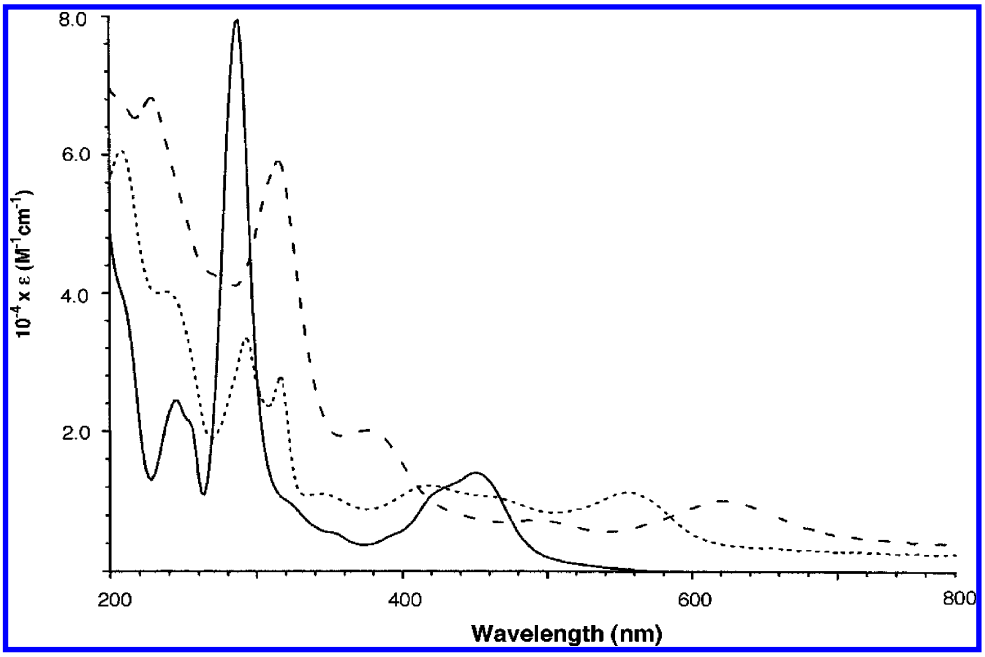

Figure 6. Absorption spectra of $[Ru((4,4'\text{-}COOEt)_2bpy)(dpb)(dtc)\}^+$ (- - -), $[Ru(4,4'\text{-}COOEt)_2bpy)((4,4'\text{-}Me)_2bpy)(dtc)]^+$ (···), and $[Ru(bpy)_3]^{2+}$ (—) in CH_3CN at room temperature.

λ is the sum of the reorganization energies for the solvent, λ_o, and intramolecular vibrations treated classically, λ_i. Assuming the solvent to be a dielectric continuum, with the ground-to-excited-state absorption approximated as creating a dipole in a sphere, gives the expression for λ_o in eq 8. In this expression, a is the radius of a sphere enclosing the molecule, D_s and D_{op} are the static and optical dielectric constants of the solvent, and $\boldsymbol{\mu}_g$ and $\boldsymbol{\mu}_e$ are the point dipole vectors of the ground and excited states, respectively.[92]

$$\lambda_o = \frac{1}{a^3}(\vec{\mu}_g - \vec{\mu}_e)^2\left(\frac{D_s - 1}{2D_s + 1} - \frac{D_{op} - 1}{2D_{op} + 1}\right) \qquad (8)$$

The solvent is a major contributor to λ and the bandwidth. Its contribution increases as the dipole moment change increases, the molecular radius decreases, and the solvent polarity increases.

The solvent dependence of E_{abs} also includes the solvent-dependent part of $\Delta G°$, $\Delta w(D_s)$, which varies with the static dielectric constant of the solvent, as shown in eq 9.

$$\Delta w(D_s) = \frac{1}{a^3}(\vec{\mu}_g{}^2 - \vec{\mu}_e{}^2)\frac{D_s - 1}{2D_s + 1} \qquad (9)$$

$[Ru(bpy)_3]^{2+}$ is of D_3 symmetry in the ground state, and $\boldsymbol{\mu}_g = 0$. The difference in E_{abs} between solvents, ΔE_{abs}, is given in eq 10. Experimentally, E_{abs} has been found to vary with D_{op}, as predicted by eq 10 from $E_{abs} = 21\,200$ cm^{-1} in nitrobenzene to 22 200 cm^{-1} in H_2O. These results were in agreement with charge transfer to a single ligand, $[Ru^{II}(bpy)_3]^{2+} + h\nu \rightarrow [Ru^{III}(bpy^{\bullet -})(bpy)_2]^{2+*}$, rather than to an orbital delocalized over all three, $[Ru^{II}(bpy)_3]^{2+} + h\nu \rightarrow [Ru^{III}(bpy^{\bullet 1/3-})_3]^{2+}$.[93]

$$\Delta E_{abs} = \frac{\vec{\mu}_e{}^2}{a^3}\left(\frac{1 - D_{op}}{2D_{op} + 1}\right) \qquad (10)$$

For low-frequency vibrations, which can be treated classically as harmonic oscillators, λ_i is given by the sum in eq 11. It is over all coupled vibrations j, those for which there is a distortion between the ground and excited states with $\Delta Q_e \neq 0$. ΔQ_e is the distortion, the change in equilibrium displacement of the normal mode between states, f_j is the force constant, S_j is the electron−vibrational coupling constant, or Huang−Rhys factor, and $\hbar\omega$ ($=h\nu$) is the vibrational quantum spacing. According to eq 11, λ_i increases as S and $\hbar\omega$ increase. S is related to ΔQ_e, the angular frequency ($\omega = 2\pi\nu$), and the reduced mass, M, as shown in eq 11a.

$$\lambda_i = \sum_j \frac{1}{2} f_j(\Delta Q_{e,j})^2 = \sum_j S_j \hbar\omega_j \qquad (11)$$

$$S_j = \frac{1}{2}\left(\frac{M_j\omega_j}{\hbar}\right)(\Delta Q_{e,j})^2 \qquad (11a)$$

Typically, MLCT absorption spectra at room temperature consist of a series of relatively featureless, broad absorption bands with the underlying vibronic components obscured; note Figure 6. This is due to overlapping bands and bandwidths comparable to or larger than the vibrational spacings. Vibronic structure can be observed at low temperatures as bandwidths narrow (eq 7).[78,81−87,89] They are included in the band-shape equations as a sum over vibronic components. This is discussed for emission band shapes in section III.C.(i).[76,77,79]

For $[Ru(bpy)_3]^{2+}$, there are 7−8 ν(bpy) ring-stretching vibrations from 1200 to 1600 cm^{-1} coupled to MLCT

(91) Anderson, P. A.; Strouse, G. F.; Treadway, J. A.; Keene, F. R.; Meyer, T. J. *Inorg. Chem.* **1994**, *33*, 3863.
(92) Chen, P.; Meyer, T. J. *Chem. Rev.* **1998**, *98*, 1439.
(93) Kober, E. M.; Sullivan, B. P.; Meyer, T. J. *Inorg. Chem.* **1984**, *23*, 2098.

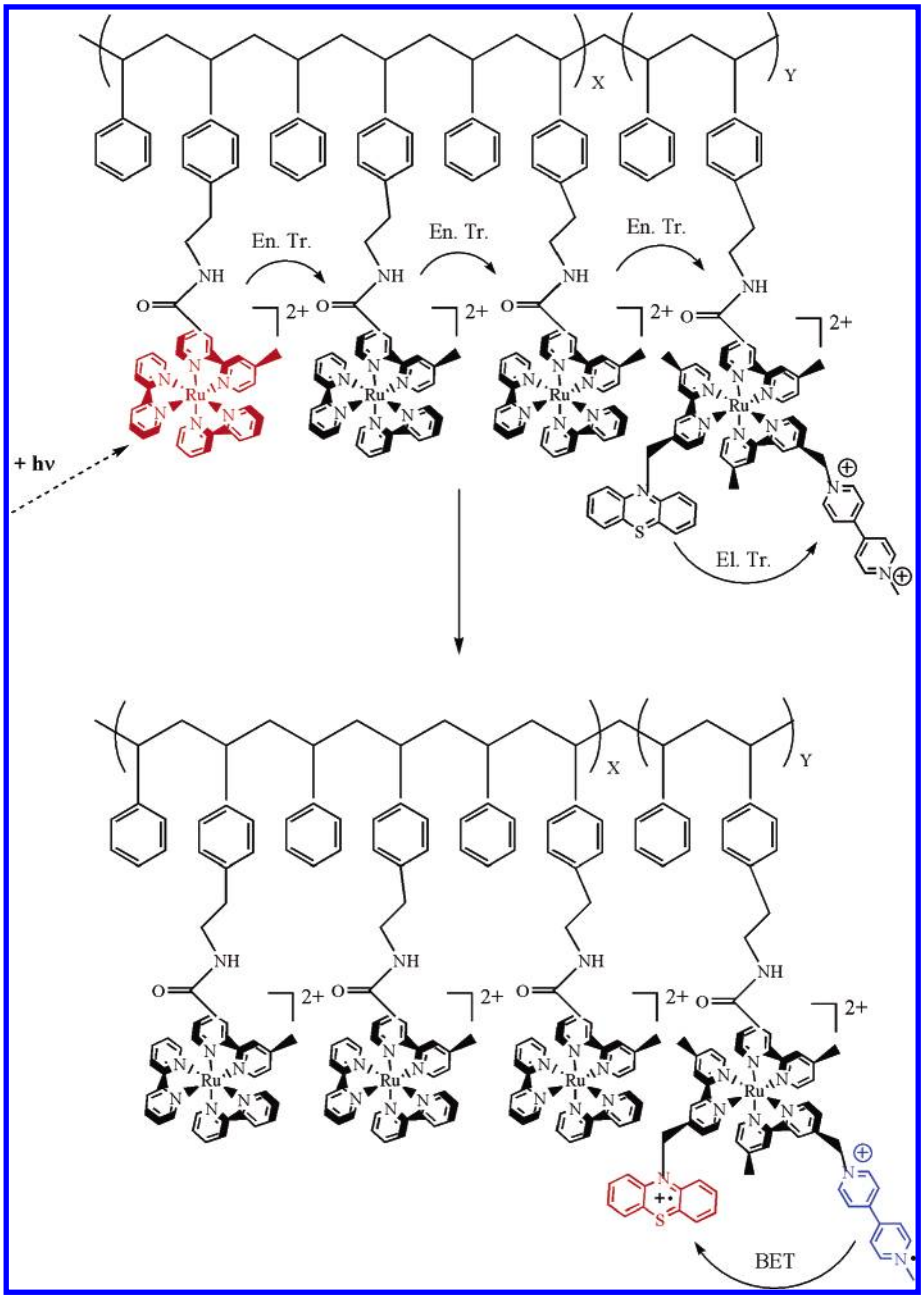

Figure 7. Derivatized PS, antenna−reaction center polymer illustrating sensitized electron transfer following MLCT excitation at a Ru^{II} antenna site.[95]

absorption. They are sufficiently close in energy that they can be treated as a single averaged mode at ~1300 cm^{-1} even at 77 K.

With the exception of transition-metal, lanthanide, and actinide complexes, most molecules are spin singlets in the ground state (S_0, $S = 0$), and absorption bands of high absorptivity appear in the spectra from transitions from S_0 to singlet excited states, S_1, S_2, ..., S_n. Transitions between states of different spin multiplicity, e.g., S → T, with T a triplet state, are weak or not observed. Spin−orbit coupling mixes these states, imparting allowedness to the transitions.

This is an important effect for second- and third-row transition-metal complexes. In the visible absorption spectrum of $[Ru(bpy)_3]^{2+}$, a $S_0 \rightarrow T$ absorption is observed on the low-energy side of the $S_0 \rightarrow S_1$ absorption at 452 nm, which is lower in absorptivity by a factor of ~10 (Figure 6). These low-energy absorptions are far more pronounced for $[Os(bpy)_3]^{2+}$ because of the larger spin−orbit coupling constant, $\xi(Os^{III})$ ~ 3000 cm^{-1} compared to ~1000 cm^{-1} for Ru(III).[57−59,78,82,84−89] Spin−orbit coupling mixes states of different spin multiplicities.

(ii) Antenna Effect. Energy Transfer. Absorbing a significant fraction of the solar irradiance (moles of incident photons per unit time) requires multilayers of individual chromophores or antenna sensitization. Antenna arrays can both broaden the region of high light absorptivity to higher energy and increase the effective molecular absorptivity. Following excitation of the antenna, the excited-state energy is transferred to a low-energy "reaction center" where, as shown schematically in Figure 1, electron transfer occurs. Energy in excess of $\Delta G_{ES}°$ for the reaction center is

dissipated as heat. As for electron transfer, energy transfer is driven by favorable free-energy gradients.

Elaborate antenna arrays are utilized in natural photosynthesis. In photosystem II, there are six chlorophyll *a*'s and one or two β-carotenes. In photosystem I, there is an integral antenna system consisting of ~90 Chl molecules and 22 carotenoids in a precisely laid out geometry.[24,26] Application of ultrafast spectroscopies and a recent theoretical treatment by Fleming and co-workers have given detailed insight into antenna dynamics and the electronic and vibrational couplings that lead to rapid, efficient energy transfer to the reaction center.[35−37,95]

Antenna arrays have been constructed from chemically linked porphyrins, organic chromophores, and dendrimers.[2,94,96−98] A derivatized polystyrene (PS) example is shown in Figure 7,[97] in which excitation of a Ru(bpy) "antenna" site is followed by facile energy transfer to a (PTZ)$Ru^{II}(MV^{2+})$ "reaction center" mimic. Energy transfer causes chromophore sensitization and electron transfer, $-Ru^{II}*(PTZ)Ru^{II}(MV^{2+})- \rightarrow -Ru^{II}(PTZ)Ru^{II}*(MV^{2+})- \rightarrow -Ru^{II}(PTZ^{\bullet+})Ru^{II}(MV^{\bullet+})$, to give a 1.15-eV redox-separated state based on $PTZ^{\bullet+}$ and $MV^{\bullet+}$.[97]

Successful light harvesting and application of the antenna effect rely on efficient light collection, energy transfer, and sensitized electron transfer. All must be rapid compared to the lifetime of the antenna molecular excited state(s).

The principles of energy transfer are well understood.[99−103] Application of time-dependent perturbation theory gives the expression in eq 12 for the energy-transfer rate constant, k_{en}. In eq 12, H is the operator that mixes the electronic wave function for the energy-transfer acceptor (ψ_{el}') and donor (ψ_{el}). The associated spin wave functions are ψ_s' and ψ_s. The total vibrational wave functions for the two states including solvent are ψ_{vib}' and ψ_{vib}.

$$k_{en} = 2\pi/\hbar\langle\psi_{el}'|H|\psi_{el}\rangle^2\langle\psi_s'|\psi_s\rangle^2\langle\psi_{vib}'|\psi_{vib}\rangle^2 = 2\pi/\hbar V_{en}^2 F_{calc} \quad (12)$$

There are two mechanisms for energy transfer. In the Förster mechanism, energy transfer is induced by an electrostatic dipole interaction between the electrons in the initial and final states. V_{en}^2 varies as $1/R^6$ with R the internuclear separation distance between donor and acceptor.

In Dexter transfer, an electrostatic perturbation mixes the electronic wave functions and V_{en}^2 varies as $\exp[-(R/L)]$. L is the sum of the average Bohr radii for the donor and acceptor. The $1/R^6$ dependence for Förster transfer, compared to the exponential dependence for Dexter transfer, favors Förster transfer at long distances. Experimentally, V_{en} values of $1-25\ cm^{-1}$ have been reported for Dexter transfer.[48,104−106]

In both Förster and Dexter transfer, the electronic wave functions include ψ_s and ψ_s'. The operator inducing energy transfer does not include spin, and in the absence of spin−orbit coupling, energy transfer can only occur between states of the same spin multiplicity. For example, $\langle\psi_s'|\psi_s\rangle = 1$ for $S \rightarrow S'$ transfer and $\langle\psi_s'|\psi_s\rangle = 0$ for $S \rightarrow T$ transfer. Spin−orbit coupling mixes the spin character of the states, making spin changes possible but still greatly decreasing the magnitude of V.

The vibrational overlap term in eq 13, F_{calc}, can be evaluated from the emission spectrum of the donor and absorption spectrum of the acceptor by use of the spectral overlap integrals in eq 13. In eq 13, $f_d(E)$ is the normalized emission spectrum of the donor and $F_a(E)$ is the normalized absorption spectrum of the acceptor. The integration is over the energy ranges of the absorption and emission spectra.[107]

$$F_{calc} = \int \frac{f_d(E)\, F_a(E)}{E^4}\, \delta E \quad (13)$$

As for nonradiative decay and electron transfer, in sections III.C.(ii) and IV, it is also possible to express F_{calc} and k_{en} in terms of specific contributions from coupled vibrations and the solvent at the donor and acceptor and the free-energy change, $\Delta G°$. These parameters can be obtained by analyzing emission band shapes or Raman excitation profiles.[83,108]

Antenna energy transfer has been demonstrated and treated quantitatively in a series of derivatized PS polymers and, as shown in Figure 7, used to sensitize electron transfer at an artificial reaction center.[34,48,94,97,109] In the PS polymers, the molecular volumes of the complexes are large relative to the repeat unit of the polymer (note Figure 10 below), which ensures an extended, rodlike structure and one-dimensional, intrastrand energy migration.

The energy-transfer experiments were conducted on mixed polymers containing both Ru^{II}(bpy) "antenna" sites, which were in the majority, and minority Os^{II}(bpy) trap sites. The energy of the Os^{II} acceptor is 1.70 eV, with $Ru^{II}* \rightarrow Os^{II}$ energy transfer favored by 0.40 eV. Antenna sensitization of $Os^{II}*$ following excitation at Ru^{II} can be highly efficient, >90%, depending on the chemical links from the metal complexes to the polymer backbone.[34]

(94) Fleming, C. N.; Maxwell, K. A.; DeSimone, J. M.; Meyer, T. J.; Papanikolas, J. M. *J. Am. Chem. Soc.* **2001**, *123*, 10336.
(95) (a) Yang, M.; Damjanovic, A.; Vaswani, H. M.; Fleming, G. R. *Biophys. J.* **2003**, *85*, 140. (b) Jordanides, X. J.; Scholes, G. D.; Shapley, W. A.; Reimers, J. R.; Fleming, G. R. *J. Phys. Chem. B.* **2004**, *108*, 1753. (c) Brixner, T.; Stenger, J.; Vaswani, H. M.; Cho, M.; Blankenship, R. E.; Fleming, G. R. *Nature* **2005**, *434*, 625.
(96) Balzani, V.; Ceroni, P.; Maestri, M.; Vicinelli, V. *Curr. Opin. Chem. Biol.* **2003**, *7*, 657.
(97) Maxwell, K. A.; Sykora, M.; DeSimone, J. M.; Meyer, T. J. *Proc. Natl. Acad. Sci. U.S.A.* **2000**, *97*, 7687.
(98) Rybtchinski, B.; Sinks, L. E.; Wasielewski, M. R. *J. Am. Chem. Soc.* **2004**, *126*, 12268.
(99) Dexter, D. L. *J. Chem. Phys.* **1953**, *21*, 836.
(100) Ulstrup, J.; Jortner, J. *J. Chem. Phys.* **1975**, *63*, 4358.
(101) Kestner, N. R.; Logan, J.; Jortner, J. *J. Phys. Chem.* **1974**, *78*, 2148.
(102) Jortner, J. *J. Chem. Phys.* **1976**, *64*, 4860.
(103) Ulstrup, J. *Charge-Transfer Processes in Condensed Media, Lecture Notes in Chemistry*; Springer-Verlag: New York, 1979.
(104) Harriman, A.; Romero, F. M.; Ziessel, R.; Benniston, A. C. *J. Phys. Chem. A* **1999**, *103*, 5399.
(105) Shaw, J. R.; Sadler, G. S.; Wacholtz, W. F.; Ryu, C. K.; Schmehl, R. H. *New J. Chem.* **1996**, *20*, 749.
(106) De Cola, L.; Balzani, V.; Barigelletti, F.; Flamigni, L.; Belser, P.; von Zelewsky, A.; Frank, M.; Voegtle, F. *Inorg. Chem.* **1993**, *32*, 5228.
(107) Naqvi, K. R.; Steel, C. *Spectrosc. Lett.* **1993**, *26*, 1761.
(108) Murtaza, Z.; Graff, D. K.; Zipp, A. P.; Worl, L. A.; Jones, W. E., Jr.; Bates, W. D.; Meyer, T. J. *J. Phys. Chem.* **1994**, *98*, 10504.
(109) Fleming, C. N.; Dupray, L. M.; Papanikolas, J. M.; Meyer, T. J. *J. Phys. Chem. A* **2002**, *106*, 2328.

Scheme 4. Kinetic Pathways Leading to Intrastrand Excited-State Energy Transfer[a]

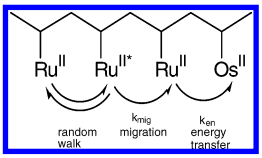

[a] The two distinct pathways shown are energy migration ($Ru^{II}* \rightarrow Ru^{II}$) and energy transfer ($Ru^{II}* \rightarrow Os^{II}$). Randon walk is the sum of migration pathways both toward and away from the Os^{II} trap site.

Analysis of the emission lifetime data revealed a complex energy-transfer mechanism in the polymers based on (1) $Ru^{II}* \rightarrow Ru^{II}$ energy migration by site-to-site hopping ($k_{migration}$ in Scheme 4), (2) long-range, random-walk energy migration along the polymer strands, and (3) $Ru^{II}* \rightarrow Os^{II}$ energy transfer. The antenna effect is efficient because energy migration is rapid (nanosecond time scale) compared to the excited-state lifetime of ~ 1 μs.[109]

Cross-surface, two-dimensional antenna sensitization has been demonstrated on ZrO_2 nanoparticles containing coadsorbed $[Os^{II}(bpy)_2(4,4'\text{-}(COOH)_2bpy)](PF_6)_2$ and $[Ru^{II}(bpy)_2(4,4'\text{-}(PO(OH)_2)_2bpy)](Br)_2$. The average rate constant for cross-surface energy transfer, $\langle k_{en} \rangle$, was found to vary exponentially with distance, consistent with Dexter transfer with an average, close-contact rate constant of $\langle k_{en} \rangle = 2.7 \times 10^7$ s^{-1}. Energy transfer occurs by long-range, cross-surface, random-walk energy migration at low surface coverages and by percolation chain transfer at high coverages.[110]

III.C. Excited States. From the Franck−Condon principle, light absorption is rapid on the time scale for nuclear motions. This means that an excited state formed by excitation is initially in the equilibrium coordinates and solvent configuration of the ground state. Subsequent relaxation to the equilibrium coordinates and configuration of the excited state occurs in tens of femtoseconds for the coupled vibrations and in picoseconds for the solvent.[111−115]

As noted above, the $[Ru(bpy)_3]^{2+}$ absorption spectrum is dominated by multiple MLCT and $\pi \rightarrow \pi^*$ absorptions that occur from the singlet ground state, ($d\pi^6$) S_0, to excited states of increasing energy, $S_0 \rightarrow S_1$, S_2, ..., S_n.[81,82] Subsequent relaxation occurs on the subpicosecond time scale to and through the lowest singlet state, S_1, to the lowest triplet ($^3(d\pi^5\pi^{*1})$ T_1), which is largely responsible for the observed excited-state properties.[111,112]

As noted above, T_1 is split by low symmetry and spin−orbit coupling into three closely spaced states separated by 30 cm^{-1}. They behave kinetically as a single state at room temperature. Transient IR and transient resonance Raman measurements have shown that the excited electron is localized on a single bpy ligand, $[Ru^{III}(bpy^{-\bullet})(bpy)_2]^{2+}*$, rather than delocalized over all three, $[Ru^{III}(bpy^{\bullet 1/3-})_3]^{2+}*$, in the thermally equilibrated excited state.[116,117]

The results of transient polarization measurements are consistent with the excited electron hopping among ligands (or rather combined electron−electron hole transfer leading to rotation of the excited-state dipole)[34] within a few picoseconds.[118,119] In the lowest triplet state $^3(d\pi^5\pi^{*1})$, the hole in the $d\pi^5$ core resides in the $d\pi$ orbital lying along the reduced bpy ligand. Rapid rotation of the excited electron between ligands is important in assemblies such as the one shown in Figure 4 in order to ensure that the excited electron is available at all three ligands regardless of which is initially involved in the excitation.

(i) Radiative Decay. Excited states decay by a combination of radiative (emissive) and nonradiative decay or undergo chemical change. The rate constant for *radiative decay*, k_r, varies with the transition moment, **M**, and the inverse cube of the average emission energy, $\langle \bar{\nu}^{-3} \rangle^{-1}$, as shown in eq 14. The transition moment is related to the transition dipole, $\boldsymbol{\mu}$, by $\mathbf{M} = e\boldsymbol{\mu}$. For transitions between states of common spin parentage, e.g., $S_1 \rightarrow S_0$, $\boldsymbol{\mu}$ is relatively large and k_r rapid because it scales with $\boldsymbol{\mu}^2$. Radiative decay typically occurs on the nanosecond time scale for organic $\pi\pi^*$ singlets, consistent with the high absorptivities of the intense $S_0 \rightarrow S_1$ absorption bands that appear in their spectra.

$$k_r = \frac{64\pi^4 n^3}{3\hbar} |\mathbf{M}|^2 \langle \bar{\nu}^{-3} \rangle^{-1} \qquad (14)$$

Radiative decay is far slower for excited-state triplets because of the spin change involved in a $T_1 \rightarrow S_0$ transition. The latter can occur on the seconds time scale. Radiative lifetimes for transition-metal complex excited states undergoing spin changes can be far shorter because spin−orbit coupling mixes singlet character into excited states of higher spin multiplicity. For example, $k_r = 3 \times 10^4$ s^{-1} for the $T_1 \rightarrow S_0$ radiative transition in $[Os(bpy)_3]^{2+}*$.[83,120]

Radiative decay results in emission. The relationship between absorption and emission is illustrated in Figure 8, assuming that they interrelate the same two states. In the case of $[Ru(bpy)_3]^{2+}$, these are S_0 and T_1. In Figure 8, E_{em} and E_{abs} are the energies of the emission and absorption maxima and λ the reorganization energy as defined previously. Gaussian band shapes are assumed in the classical limit with $h\nu_{vib} = h\nu_{vib}'$ for the coupled vibrations and solvent.

Figure 8 shows that the red shifts observed for emission compared to absorption are a natural consequence of the Franck−Condon principle. The change in the electronic

(110) Trammell, S. A.; Yang, J.; Sykora, M.; Fleming, C. N.; Odobel, F.; Meyer, T. J. *J. Phys. Chem. B* **2001**, *105*, 8895.
(111) McCusker, J. K. *Acc. Chem. Res.* **2003**, *36*, 876.
(112) Damrauer, N. H.; Cerullo, G.; Yeh, A.; Boussie, T. R.; Shank, C. V.; McCusker, J. K. *Science* **1997**, *275*, 54.
(113) Horng, M. L.; Gardecki, J. A.; Papazyan, A.; Maroncelli, M. *J. Phys. Chem.* **1995**, *99*, 17311.
(114) Barbara, P. F.; Meyer, T. J.; Ratner, M. A. *J. Phys. Chem.* **1996**, *100*, 13148.
(115) Kahlow, M. A.; Kang, T. J.; Barbara, P. F. *J. Phys. Chem.* **1987**, *91*, 6452.
(116) Omberg, K. M.; Schonover, J. R.; Treadway, J. A.; Leasure, R. M.; Dyer, R. B.; Meyer, T. J. *J. Am. Chem. Soc.* **1997**, *119*, 7013.
(117) Dallinger, R. F.; Woodruff, W. H. *J. Am. Chem. Soc.* **1979**, *101*, 4391.
(118) Shaw, G. B.; Brown, C. L.; Papanikolas, J. M. *J. Phys. Chem. A* **2002**, *106*, 1483.
(119) Wallin, S.; Davidsson, J.; Modin, J.; Hammarström, L. *J. Phys. Chem. A* **2005**, *109*, 4697.
(120) Kober, E. M.; Caspar, J. V.; Lumpkin, R. S.; Meyer, T. J. *J. Phys. Chem.* **1986**, *90*, 3722.

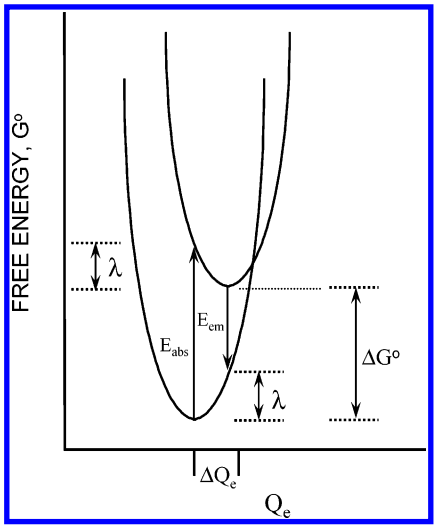

Figure 8. Schematic energy-coordinate diagram in the average mode approximation illustrating the relationship between absorption and emission. See the text.

configuration between ground and excited states causes changes both in the intramolecular structure and in the surrounding medium. Light absorption occurs rapidly on the time scale for nuclear motions and gives the excited state initially in the nuclear configurations of the ground state. Similarly, emission from the thermally equilibrated excited state occurs to nonequilibrium nuclear configurations in the ground state.

In the classical limit with $h\nu_{vib} = h\nu_{vib}'$, E_{em} is related to λ, $\Delta G°$, and E_{abs} as shown in eq 15. In eq 15, the spectroscopic quantities E_{em} and E_{abs} are related to the free-energy difference between states, $\Delta G°$, rather than to the internal energy difference, $\Delta E°$. This has been shown to be the case based on both a classical free-energy surface analysis[121] and a quantum mechanical, harmonic oscillator analysis in the limit of small frequency changes.[122]

$$E_{em} = \Delta G° - \lambda \tag{15a}$$

$$E_{abs} - E_{em} = 2\lambda \tag{15b}$$

Because emission typically occurs from a single state, analysis of emission spectral profiles is far simpler than for absorption, where there are usually complications from overlapping bands; note Figure 6. At temperatures below ambient, vibronic structure appears in the emission spectrum of $[Ru(bpy)_3]^{2+*}$, arising from 7−8 coupled ν(bpy) ring stretching vibrations from 1200 to 1600 cm^{-1}. They appear as a single, unresolved progression at ~1300 cm^{-1} at 77 K,[57,83,117,120] with further resolution into the separate components at lower temperatures.[84−87]

Emission Spectral Fitting. MLCT emission spectra have been fit by mode averaging and straightforward line-shape equations[76,77,83,92,120,122] and the excited states investigated by transient resonance Raman and infrared spectroscopies.[117,123−127]

In the average-mode approximation, the coupled ν(bpy) vibrations are treated as an average harmonic oscillator, with S defined as the sum in eq 16a and $\hbar\omega$ the weighted average in eq 16b. The summations are over the coupled vibrations within a limited range of frequencies, as noted above from ~1200−1600 cm^{-1} for the ν(bpy) vibrations.

$$S = \sum_j S_j \tag{16a}$$

$$\hbar\omega = \sum_j S_j \hbar\omega_j / \sum_j S_j \tag{16b}$$

The spectra are constructed from a series of vibronic lines separated by vibrational spacing, $\hbar\omega = h\nu$, with ω the angular frequency $= 2\pi\nu$. Relative heights are a function of the electron−vibrational coupling constant S and vary as $S^{\upsilon}/\upsilon!$. The bandwidth of each vibronic component includes both the solvent reorganization energy, λ_o (eq 8), and the reorganization energy from low-frequency modes treated classically, $\lambda_{i,L}$ (eq 11a); note eq 17b below.

Analysis of emission spectral profiles gives (1) E_o, the energy of the $\upsilon = 0 \rightarrow \upsilon' = 0$ vibronic band, the *energy gap*, (2) $\Delta\bar{\nu}_{1/2}$, the bandwidth at half-maximum for each vibronic band, and (3) S and $\hbar\omega$. These parameters characterize the excited state: (1) S is a measure of ΔQ_e and the extent of excited-state distortion in the acceptor ligand.[122,128] (2) E_o is related to $\Delta G_{ES}°$, as shown in eq 17a. (3) $\Delta\bar{\nu}_{1/2}$ gives $\lambda_{o,L}$ (eqs 7 and 17b). (4) The relative rate constants for nonradiative decay can be calculated from E_o, S, and $\lambda_{o,L}$; see below. From an emission spectral fitting of $[Ru(bpy)_3]^{2+*}$, $S = 1.0$ with $\hbar\omega = 1300$ cm^{-1}.[83,129]

$$E_o = \Delta G_{ES}° - (\Delta\bar{\nu}_{1/2})^2/16k_BT\ln 2 \tag{17a}$$

$$\lambda_{o,L} = \lambda_o + \lambda_{i,L} \tag{17b}$$

(ii) Nonradiative Decay. In *nonradiative decay*, the transition between excited and ground states is induced by "promoting modes", which have the symmetry properties required to mix the electronic wave functions of the initial and final states. The excess energy when nonradiative decay occurs is channeled into "acceptor" modes and the solvent. The acceptor modes are typically high- or medium-frequency vibrations for which $\Delta Q_e \neq 0$.

Nonradiative decay occurs through a series of channels from a discrete set of vibrational levels, υ, in the excited state to final levels υ' in the ground state. Expressions for k_{nr} have been derived from time-dependent perturbation theory.[120,130−136] In the limiting case of a single coupled

(121) Marcus, R. A.; Sutin, N. *Inorg. Chem. Commun.* **1986**, *5*, 119.
(122) Hupp, J. T.; Neyhart, G. A.; Meyer, T. J.; Kober, E. M. *J. Phys. Chem.* **1992**, *96*, 10820.
(123) Turner, J. J.; George, M. W.; Johnson, F. P. A.; Westwell, J. R. *Coord. Chem. Rev.* **1993**, *93*, 101.
(124) Glyn, P.; George, M. W.; Hodges, P. M.; Turner, J. J. *J. Chem. Soc., Chem. Commun.* **1989**, *21*, 1655.
(125) Schoonover, J. R.; Bignozzi, C. A.; Meyer, T. J. *Coord. Chem. Rev.* **1997**, *165*, 239.
(126) Schoonover, J. R.; Strouse, G. F. *Chem. Rev.* **1998**, *98*, 1335.
(127) Dattelbaum, D. M.; Meyer, T. J. *J. Phys. Chem. A* **2002**, *106*, 4519.
(128) Caspar, J. V.; Westmoreland, T. D.; Allen, G. H.; Bradley, P. G.; Meyer, T. J.; Woodruff, W. H. *J. Am. Chem. Soc.* **1984**, *106*, 3492.
(129) Claude, J. P. *Photophysics of polypyridyl complexes of Ru(II), Os-(II), and Re(I)*; Univeristy of North Carolina at Chapel Hill: Chapel Hill, NC, 1995.
(130) Freed, K. F.; Jortner, J. *J. Chem. Phys.* **1970**, *52*, 6272.

vibration, or average vibration (eq 16), the contribution to k_{nr} from the $\upsilon = 0 \rightarrow \upsilon'$ channel, $k_{nr}(\upsilon = 0 \rightarrow \upsilon')$, is given by eq 18, with $|\Delta G^\circ| = \Delta G_{ES}^\circ$. This expression assumes that $\hbar\omega \gg k_BT$ ($k_BT = 200$ cm^{-1} at 25 °C) so that only the $\upsilon = 0$ level in the excited state is appreciably populated and contributes to nonradiative decay. The term $\lambda_{o,L}$ is the sum of the solvent reorganization energy and coupled low-frequency vibrations treated classically (eq 17b).

$$k_{nr}(\upsilon = 0 \rightarrow \upsilon') = \frac{2\pi}{\hbar}\frac{V_k^{\,2}}{\sqrt{4\pi RT\lambda_{o,L}}}\langle\psi_{vib}(\upsilon')\,\psi_{vib}(\upsilon = 0)\rangle^2\frac{S^{\upsilon'}}{\upsilon'!} \times \exp\left[\frac{(|\Delta G^\circ| - \upsilon\hbar\omega - \lambda_{o,L})^2}{4\lambda_{o,L}RT}\right] \quad (18)$$

$k_{nr}(\upsilon = 0 \rightarrow \upsilon')$ is the product of three terms:

(1) *The preexponential* term contains both the barrier crossing frequency, $2\pi V_k^2/\hbar$, and the classical density of states in the coupled solvent and low-frequency vibrational modes, $(4\pi RT\lambda_{o,L})^{-1/2}$. V_k is the vibrationally induced electronic coupling matrix element for the promoting mode(s). V_k is defined in eq 19 for a single mode of reduced mass M_k, quantum spacing $\hbar\omega_k$, and normal coordinate Q_k.

$$V_k = \frac{\hbar^2}{M_k}\langle\psi_{el}'|\delta/\delta Q_k|\psi_{el}\rangle\langle\psi_{vib}'|\delta/\delta Q_k|\psi_{vib}\rangle = \frac{\hbar}{\sqrt{M_k}} \times \langle\psi_{el}'|\delta/\delta Q_k|\psi_{el}\rangle\sqrt{\hbar\omega_k/2} = C_k\sqrt{\hbar\omega_k/2} \quad (19)$$

(2) *The square of the vibrational overlap integral* with $\langle\psi_{vib}'(\upsilon')|\psi_{vib}(\upsilon{=}0)\rangle^2 = (S^{\upsilon'}/\upsilon'!)\exp(-S')$ for a harmonic oscillator. It gives the extent to which the vibrational coordinates in the initial and final vibrational levels are coincident along normal coordinate Q. Vibrational overlap is illustrated in Figure 10 for electron transfer in the inverted region. The transition between ψ_{vib} and ψ_{vib}' is referred to as nuclear tunneling in the physics literature. It is a quantum effect arising from the probabilistic uncertainty in spatial coordinates for particles at the quantum level.

(3) *The classical barrier crossing*, $\exp\{-[(\Delta G^\circ(\upsilon,\upsilon') - \lambda_{o,L})^2/4\lambda_{o,L}RT]\}$, includes contributions from all other coupled vibrations treated classically and the solvent. It gives the fraction of molecules at temperature T at the barrier crossing in each of the coupled low-frequency vibrations and the solvent. It ensures that the $\upsilon \rightarrow \upsilon'$ channel occurs with energy conservation.

As shown in eq 20, k_{nr} is the sum over all channels, $k_{nr} = \sum_{\upsilon'}k_{nr}(\upsilon)'$. This result can be generalized to include any number of coupled vibrations, levels above $\upsilon = 0$, and $\hbar\omega \neq \hbar\omega'$.[83,92,120,130−136]

$$k_{nr} = \frac{2\pi}{\hbar}\frac{V_k^{\,2}}{\sqrt{4\pi\lambda_{o,L}RT}}\sum_{\upsilon'}\exp(-S)\frac{S^{\upsilon'}}{\upsilon'!} \times \exp\left\{-\left[\frac{(|\Delta G^\circ| - \upsilon\hbar\omega - \lambda_{o,L})^2}{4\lambda_{o,L}RT}\right]\right\} \quad (20)$$

In the limits E_o ($=|\Delta G^\circ| - \lambda_{o,L}$) $\gg S\hbar\omega$ and $\hbar\omega \gg k_BT$, k_{nr} is given by the famous "energy gap law" in eq 21.[130−136] This result illustrates the central role of the energy gap in nonradiative decay.[120]

$$k_{nr} = \frac{\sqrt{\pi}\omega_k C_k^{\,2}}{\sqrt{2\hbar\omega E_o}}\exp\left[-S - \frac{\gamma E_o}{\hbar\omega} + \left(\frac{\gamma + 1}{\hbar\omega}\right)^2\lambda_{o,L}k_BT\right] \quad (21a)$$

$$\gamma = \ln(E_o/S\hbar\omega) - 1 \quad (21b)$$

All of the parameters in eq 21 except C_k are available from emission spectral fitting. This has allowed quantitative application of the energy gap law to nonradiative decay for Ru(II), Os(II), and Re(I) MLCT excited states.[57,83,92,120,127,137]

A more inclusive treatment with S and $\hbar\omega$ values included for all coupled vibrations on a mode-by-mode basis acquired by the analysis of Raman excitation profiles has also been applied to MLCT excited states.[83,138−141]

(iii) Excited-State Lifetimes and Reactivity. In the absence of chemical reactions, excited states decay by a combination of radiative and nonradiative decay with lifetimes, τ, related to k_r and k_{nr} as in eq 22a. The emission quantum yield in eq 22b is defined as $\Phi_{em} = k_r/(k_r + k_{nr})$.

$$\tau^{-1} = k_r + k_{nr} \quad (22a)$$

$$k_r = \Phi_{em}\tau^{-1} \quad (22b)$$

Many MLCT excited-state properties are predictable based on this result and those in previous sections. The energy gap is a key parameter. It defines emission and low-energy absorption maxima and excited-state redox potentials. It also helps to determine τ, with k_r varying as E_o^{-3} (eq 14) and k_{nr} as $\exp(-E_o)$ (eq 20).[142]

Variations in the surrounding ligands have been used to vary E_o and τ systematically to demonstrate the validity of the energy gap law.[83,92,120,129,137,142] There are other ways to manipulate τ. As predicted by eq 21, k_{nr} should decrease and τ increase if S is decreased. This can be accomplished by enhanced electronic delocalization of the excited electron in the acceptor ligand, which has the effect of decreasing structural changes. Enhanced rigidity has been shown to have the same effect.[91,142−144]

(131) Bixon, M.; Jortner, J.; Cortes, J.; Heitele, H.; Michel-Beyerle, M. E. *J. Phys. Chem.* **1994**, *98*, 7289.
(132) Bixon, M.; Jortner, J. *J. Chem. Phys.* **1968**, *48*, 715.
(133) Englman, R.; Jortner, J. *J. Mol. Phys.* **1970**, *18*, 145.
(134) Lin, S. H. Some considerations of theory and experiment in ultrafast processes. *Radiationless Transitions*; Academic: New York, 1980.
(135) Robinson, G. W.; Frosch, R. P. *J. Chem. Phys.* **1968**, *38*, 1187.
(136) Freed, K. F. *Top. Curr. Chem.* **1972**, *31*, 65.
(137) Worl, L. A.; Duesing, R.; Chen, P.; Della Ciana, L.; Meyer, T. J. *J. Chem. Soc., Dalton Trans.* **1991**, 849.
(138) Myers, A. B. *Chem. Phys.* **1994**, *180*, 215.
(139) Heller, E. J. *Acc. Chem. Res.* **1981**, *14*, 368.
(140) Zink, J. I.; Shin, K. S. K. *Adv. Photochem.* **1991**, *16*, 119.
(141) Kelly, A. M. *J. Phys. Chem. A* **1999**, *103*, 6891.
(142) Kober, E. M.; Caspar, J. V.; Sullivan, B. P.; Meyer, T. J. *Inorg. Chem.* **1988**, *27*, 4587.
(143) Treadway, J. A.; Strouse, G. F.; Ruminski, R. R.; Meyer, T. J. *Inorg. Chem.* **2001**, *40*, 4508.

Manipulation of the energy gap has led to the synthesis of "designer excited states" in which excited-state properties are manipulated systematically by varying the ligands.[57,78,80,120,137,142−144] This includes the series $[Os(bpy)(L)_4]^{n+}$ and $[Os(phen)(L)_4]^{n+}$. Variations in the nonchromophoric ligands L in this series were used to vary MLCT excited-state lifetimes from 0.041 to 4.3 μs and emission quantum yields from 0.003 to 0.44 in CH_3CN at 23 ± 2 °C as E_o varied from 13 080 to 19 790 cm^{-1}.[120,142]

In these Os complexes, metal−ligand mixing with electron-donating ligands such as Cl^- decreases E_o by increasing the energy of dπ. Ligands such as CO have the opposite effect in stabilizing dπ by d$\pi-\pi^*$(CO) back-bonding.

In the series $[Re^I(4,4'\text{-}X_2bpy)(CO)_3Cl]$, variations in X from electron donor (e.g., OMe) to electron acceptor (e.g., OOCEt) were used to vary the energy of the $\pi^*(4,4'\text{-}X_2\text{-}bpy)$ acceptor levels, with E_o varying from 14 050 to 18 100 cm^{-1}. This provides a second way to vary the energy gap systematically.[137]

MLCT emission energies and lifetimes are solvent-dependent because of the influence of the solvent on E_o and λ_o (eqs 10 and 15). Emission energies for $[Ru(bpy)_3]^{2+*}$ vary from 606 nm in dichloromethane to 630 nm in *N*,*N*-dimethylformamide at 25 °C, consistent with the dielectric continuum prediction in eq 10.[93,145]

MLCT lifetimes are weakly temperature-dependent because of the temperature dependence of E_o, which influences both k_r and k_{nr}. The temperature dependence arises from entropic differences between the excited and ground states.[146] Additional temperature effects, which arise from thermal population and decay through higher lying excited states, appear; see eq 23 below.[147,148]

Reactivity. In the new electronic configuration of an excited state, lowered barriers can open new pathways for reaction including decomposition.

(a) Ligand Loss from dd Excited States. Low-lying dd [metal-centered (MC)] excited states complicate the excited-state properties of ruthenium(II) polypyridyl complexes by contributing to nonradiative decay and causing decomposition. In these $d\pi^5 d\sigma^{*1}$ excited states, a dσ^* metal−ligand antibonding orbital (e_g in O_h symmetry) is occupied, which leads to metal−ligand bond breaking.[149−162]

The dd states are accessed by thermal activation and barrier crossing from MLCT states after they are formed by excitation. As shown by the k_2 term in eq 23, this introduces a temperature dependence into τ. There is an additional contribution to the temperature dependence arising from thermal population and decay through a fourth MLCT state, the k_1 term in eq 23. Nonradiative decay through this upper MLCT state is rapid because its enhanced singlet character causes greater mixing with the ground state.[147,148]

$$\tau^{-1} = k_0 + k_1 \exp[-(E_1/RT)] + k_2 \exp[-(E_2/RT)] \quad (23)$$

Population of dd states can lead to efficient ligand loss. For the $[Ru(bpy)_3]^{2+}$ analogue *cis*-$[Ru(bpy)_2(py)_2]^{2+}$ (py is pyridine), MLCT excitation leads to loss of a py ligand with quantum yields (the ratio of chemical events to total molecules excited) as high as 0.3. In nonpolar solvents with added anions such as NCS^-, $[Ru(bpy)_3]^{2+}$ is also photochemically unstable with a bpy ligand being replaced by ion-paired NCS^-, for example.[163]

Ligand-loss photochemistry is inhibited in rigid media[148,164−173] and at low temperatures where thermal population and decay through the dd states is unimportant (eq 23). Ligand-loss photochemistry can also be avoided by stabilizing the lowest MLCT state, as in $[Ru((4,4'\text{-}COOEt)_2bpy)(dpb)(dtc)]^+$ in Figure 6, so that the energy gap for the k_2 term in eq 23 is large.[80,91,152,164] It can be avoided in molecular assemblies for artificial photosynthesis by ensuring that the time scale for energy or electron transfer is far shorter than the time scale for thermally activated dd MLCT barrier crossing. To put this into perspective, $\tau_2^{-1} = k_2 \exp[-(E_2/RT)]$ from eq 23, with $\tau_2 \sim 0.1-0.3$ μs for $[Ru(bpy)_3]^{2+*}$ at room temperature in solution.

(144) Treadway, J. A.; Loeb, B.; Lopez, R.; Anderson, P. A.; Keene, F. R.; Meyer, T. J. *Inorg. Chem.* **1996**, *35*, 2242.
(145) Caspar, J. V.; Meyer, T. J. *J. Am. Chem. Soc.* **1983**, *105*, 5583.
(146) Claude, J. P.; Meyer, T. J. *J. Phys. Chem.* **1995**, *99*, 51.
(147) Danielson, E.; Lumpkin, R. S.; Meyer, T. J. *J. Phys. Chem.* **1987**, *91*, 1305.
(148) Lumpkin, R. S.; Kober, E. M.; Worl, L. A.; Murtaza, Z.; Meyer, T. J. *J. Phys. Chem.* **1990**, *94*, 239.
(149) Durham, B.; Caspar, J. V.; Nagle, J. K.; Meyer, T. J. *J. Am. Chem. Soc.* **1982**, *104*, 4803.
(150) Thompson, D. W.; Wishart, J. F.; Brunschwig, B. S.; Sutin, N. *J. Phys. Chem. A* **2001**, *105*, 8117.
(151) Tachiyashiki, S.; Ikezawa, H.; Mizumachi, K. *Inorg. Chem.* **1994**, *33*, 623.
(152) Rillema, D. P.; Blanton, C. B.; Shaver, R. J.; Jackman, D. C.; Boldaji, M.; Bundy, S.; Worl, L. A.; Meyer, T. J. *Inorg. Chem.* **1992**, *31*, 1600.
(153) Rillema, D. P.; Taghdiri, D. G.; Jones, D. S.; Keller, C. D.; Worl, L. A.; Meyer, T. J.; Levy, H. A. *Inorg. Chem.* **1987**, *26*, 578.
(154) Walcholtz, W. F.; Auerbach, R. A.; Schmehl, R. H. *Inorg. Chem.* **1986**, *25*, 227.
(155) Barigelletti, F.; Belser, P.; von Zelewsky, A.; Balzani, V. *J. Phys. Chem.* **1986**, *89*, 3680.
(156) Walcholtz, W. F.; Auerbach, R. A.; Schmehl, R. H.; Ollino, M.; Cherry, W. R. *Inorg. Chem.* **1985**, *24*, 1758.
(157) Juris, A.; Barigelletti, F.; Balzani, V.; Belser, P.; von Zelewsky, A. *Inorg. Chem.* **1985**, *24*, 202.
(158) Pinnick, D. V.; Durham, B. *Inorg. Chem.* **1984**, *23*, 3841.
(159) Cherry, W. R.; Henderson, L. H. *Inorg. Chem.* **1984**, *23*, 983.
(160) Henderson, L. H.; Fronczek, F.; Cherry, W. R. *J. Am. Chem. Soc.* **1984**, *106*, 5876.
(161) Allen, G. H.; White, R. P.; Rillema, D. P.; Meyer, T. J. *J. Am. Chem. Soc.* **1984**, *106*, 2613.
(162) Coe, B. J.; Friesen, D.; Thompson, D. W.; Meyer, T. J. *Inorg. Chem.* **1996**, *34*, 4575 and references cited therein.
(163) Durham, B.; Walsh, J. L.; Carter, C. L.; Meyer, T. J. *Inorg. Chem.* **1980**, *19*, 860.
(164) Adelt, M.; Devenney, M.; Meyer, T. J.; Thompson, D. W.; Treadway, J. A. *Inorg. Chem.* **1998**, *37*, 2616.
(165) Maruszewski, K.; Strommen, D. P.; Kincaid, J. R. *J. Am. Chem. Soc.* **1993**, *115*, 8345.
(166) Allsop, S. R.; Cox, A.; Kemp, T. J.; Reed, W. J. *J. Chem. Soc., Faraday Trans. 1* **1978**, *74*, 353.
(167) Allsop, S. R.; Cox, A.; Kemp, T. J.; Reed, W. J.; Carassits, V.; Traverso, O. *J. Chem. Soc., Faraday Trans. 1* **1979**, *75*, 353.
(168) Hager, G. D.; Crosby, G. A. *J. Am. Chem. Soc.* **1975**, *97*, 7031.
(169) Hecker, C. R.; Gushurst, A. K. I.; McMillin, D. R. *Inorg. Chem.* **1991**, *30*, 538.
(170) Kincaid, J. R. *Chem. Eur. J.* **2000**, *6*, 4055.
(171) Campagna, S.; Bartolotta, A.; Di Marco, G. *Chem. Phys. Lett.* **1993**, *206*, 30.
(172) Masschelein, A.; Kirsch-De Mesmaeker, A.; Willsher, C. J.; Wilkinson, F. *J. Chem. Soc., Faraday Trans.* **1991**, *87*, 259.
(173) Mongey, K. F.; Vos, J. G.; MacCraith, B. D.; McDonagh, C. M. *Coord. Chem. Rev.* **1999**, *185−186*, 417.

For most Os(II) and Re(I) complexes, dd states are not a complicating feature at least at room temperature. The splitting between the dπ and dσ* orbitals (10 *Dq*) is greater [~30% greater for Os(II)], and dd states are not significantly populated. By contrast, in related complexes of Fe(II), dd states are lowest lying or easily accessible thermally. This greatly limits their usefulness in electron- or energy-transfer applications.

(b) Other Decomposition Pathways. The chromophore $[Ru(4,4'\text{-}(COOH)_2bpy)_2(NCS)_2]$ has been one of the dyes of choice in photovoltaic applications involving Grätzel-type cells and adsorption on TiO_2. This is true even though photoinjection results in the Ru(III) form of the adsorbed complex on the surface and it is unstable with respect to intramolecular $NCS^- \rightarrow Ru^{III}$ electron transfer and release of $(NCS)_2$.[10,174,175]

Even with this instability, this adsorbed dye is stable through 10^8 redox cycles, which corresponds to 20 years of operation in natural sunlight.[10] In this case, stability is a consequence of the difference in time scales for the decomposition reaction (seconds) and re-reduction of surface-bound Ru(III) by I^- (nanoseconds) [section II.B(ii)].

IV. The Modules. Photochemical Electron Transfer

IV.A. Intramolecular Electron Transfer. The initiating event for the energy conversion reactions in Figures 1 and 2 is intra-assembly electron transfer. In the classical limit, the rate constant k_{ET} is given by eq 24.[92,100−103,176−182]

$$k_{ET} = \nu_{ET} \exp\left\{-\left[\frac{(\lambda + \Delta G^\circ)^2}{4\lambda RT}\right]\right\} \tag{24}$$

As before, λ is the sum of intramolecular, λ_i, and solvent, λ_o, reorganization energies. In this case, they pertain to electron transfer, e.g., $[Ru(bpy)_3]^{2+}$*, MV^{2+}, → $[Ru(bpy)_3]^{3+}$, MV^+, and are different from λ_i and λ_o for nonradiative decay of $[Ru(bpy)_3]^{2+}$*, for example. The free-energy dependence of k_{ET} in eq 24 has been tested for bimolecular electron-transfer quenching of $[Ru(bpy)_3]^{2+}$*. Analysis of these data also gave an estimate for the excited-state redox potentials in Scheme 2.[56,183−186] In the limit of weak electronic coupling between the electron-transfer donor and acceptor, the *nonadiabatic* limit, the barrier crossing frequency, ν_{ET}, is the electron tunneling frequency, ν_e. It is related to λ and the electron-transfer matrix element, H_{DA}, as shown in eq 25. H_{DA} is the resonance energy arising from orbital mixing between the donor and acceptor orbitals.

$$\nu_{ET} = \nu_e = \frac{2\pi H_{DA}^{\ 2}}{\hbar}\sqrt{\frac{1}{4\pi\lambda RT}} \tag{25}$$

Even with H_{DA} only tens of cm^{-1} in magnitude, electron tunneling is rapid on the time scale for nuclear motions. This is the *adiabatic* limit, in which the barrier crossing is dictated by the frequency or frequencies of the slowest coupled nuclear motion or motions, ν_n. These are typically collective dipole reorientation modes in the solvent or translation of ion-paired counterions. In this limit, ν_{ET} is given by eq 26, with ν_n the frequency of the slowest mode or an average frequency if there is more than one contributor. In the intermediate dynamic region, ν_{ET} is given by the kinetic average in eq 27.

$$\nu_{ET} = \nu_n \tag{26}$$

$$\frac{1}{\nu_{ET}} = \frac{1}{\nu_e} + \frac{1}{\nu_n} \tag{27}$$

If there is a coupled high-frequency vibration or averaged vibration with $\hbar\omega \gg k_BT$ and assuming $\hbar\omega = \hbar\omega'$, k_{ET} is given by eq 28. As before, $\lambda_{o,L}$ includes both λ_o and low-frequency modes treated classically, $\lambda_{i,L}$ (eq 11) but for electron transfer. The result in eq 28 can be fully generalized to include multiple vibrations, frequency changes, etc.[100−103,179,187−196]

$$k_{ET} = \frac{2\pi}{\hbar}\frac{H_{DA}^{\ 2}}{\sqrt{4\pi\lambda_{o,L}RT}}\sum_{v'}\exp(-S)\frac{S^{v'}}{v'!} \times \exp\left[-\frac{(\Delta G^\circ + v'\hbar\omega + \lambda_{o,L})^2}{4\lambda_{o,L}RT}\right] \tag{28}$$

If the solvent is treated as a dielectric continuum and electron transfer as occurring between spheres of radii a_1 and a_2 at an internuclear separation distance d, λ_o is given by eq 29. As before, D_s and D_{op} are the static and optical dielectric constants of the solvent.[92,103,114,176−178,187,197−201]

(174) Brown, G. M.; Callahan, R. W.; Meyer, T. J. *Inorg. Chem.* **1975**, *14*, 1915.
(175) Bond, A. M.; Deacon, G. B.; Howitt, J.; MacFarlane, D. R.; Spiccia, L.; Wolfbauer, G. *J. Electrochem. Soc.* **1999**, *146*, 648.
(176) Sutin, N. *Prog. Inorg. Chem.* **1983**, *30*, 441.
(177) Newton, M. D.; Sutin, N. *Annu. Rev. Phys. Chem.* **1984**, *35*, 437.
(178) Hush, N. S. *Coord. Chem. Rev.* **1985**, *64*, 135.
(179) Marcus, R. A.; Sutin, N. *Biochim. Biophys. Acta* **1985**, *811*, 265.
(180) Newton, M. D. *Adv. Chem. Phys.* **1999**, *106*, 303.
(181) Meyer, T. J.; Taube, H. Comprehensive Coordination Chemistry, The Synthesis, Reactions, Properties and Applications of Coordination Compounds. *Electron-Transfer Reactions*; Pergammon Press: Oxford, U.K., 1987; Vol. 1, pp 331−384.
(182) Jortner, J.; Bixon, M. *Advances in Chemical Physics, Electron Transfer—From Isolated Molecules to Biomolecules, Part One*; John Wiley & Sons: New York, 1999.
(183) Bock, C. R.; Meyer, T. J.; Whitten, D. G. *J. Am. Chem. Soc.* **1975**, *97*, 2909.
(184) Young, R. C.; Meyer, T. J.; Whitten, D. G. *J. Am. Chem. Soc.* **1975**, *97*, 4781.
(185) Rehm, D.; Weller, A. *Ber. Bunsen-Ges. Phys. Chem.* **1969**, *73*, 834.
(186) Rehm, D.; Weller, A. *Isr. J. Chem.* **1970**, *8*, 259.
(187) Levich, V. *Adv. Electrochem. Electrochem. Eng.* **1966**, *4*, 249.
(188) Bixon, M.; Jortner, J. *Faraday Discuss. Chem. Soc.* **1982**, *74*, 17.
(189) Siders, P.; Marcus, R. A. *J. Am. Chem. Soc.* **1981**, *103*, 741.
(190) Marcus, R. A. *J. Chem. Phys.* **1984**, *81*, 4494.
(191) Islampour, R.; Lin, S. H. *J. Phys. Chem.* **1991**, *95*, 10261.
(192) Islampour, R.; Alden, R. G.; Wu, G. Y. C.; Lin, S. H. *J. Phys. Chem.* **1993**, *97*, 6793.
(193) De Vault, D. *Quantum Mechanical Tunneling in Biological Systems*; Cambridge University Press: Cambridge, U.K., 1984.
(194) Efrima, S.; Bixon, M. *Chem. Phys.* **1976**, *13*, 447.
(195) Newton, M. D. *Chem. Rev.* **1991**, *91*, 767.
(196) Jortner, J.; Bixon, M. *Ber. Bunsen-Ges. Phys. Chem.* **1995**, *99*, 296.
(197) Marcus, R. A. *Annu. Rev. Phys. Chem.* **1966**, *15*, 155.
(198) Hush, N. S. *Prog. Inorg. Chem.* **1967**, *8*, 391.
(199) Dogonadze, R. R.; Kuznetsov, A. M. *Prog. Surf. Sci.* **1975**, *6*, 1.
(200) Sutin, N. *Acc. Chem. Res.* **1982**, *15*, 275.
(201) Marcus, R. A. *Rev. Mod. Phys.* **1993**, *65*, 599.

More sophisticated treatments are available by separating λ_o into components arising from orientational fluctuations of solvent dipoles and density fluctuations[202−204] and by use of frequency-resolved cavity models.[205−207]

$$\lambda_o = e^2\left(\frac{1}{2a_1} + \frac{1}{2a_2} - \frac{1}{d}\right)\left(\frac{1}{D_{op}} - \frac{1}{D_s}\right) \qquad (29)$$

Based on eq 29, the magnitude of λ_o and its contribution to the electron-transfer barrier decrease as (1) the radii of the redox sites (a_1 and a_2) increase, (2) the electron-transfer distance (d) decreases, and (3) the static dielectric constant (D_s) decreases and the optical dielectric constant (D_{op}) increases. Large reactants, small electron-transfer distances, and nonpolar solvents all increase k_{ET}.

The coupled vibrations and the extent to which they create a barrier through the $(S^v/v!)\exp(-S)$ and $\lambda_{i,L}$ terms depend on the reaction. In reductive electron-transfer quenching of $[Ru(bpy)_3]^{2+*}$, $[Ru^{III}(bpy^{\bullet-})(bpy)_2]^{2+*}$, D, $\rightarrow [Ru(bpy)_3]^{+}$, D^+, an electron is added to a $d\pi$ orbital, $d\pi^5\pi^{*1} + e^- \rightarrow d\pi^6\pi^{*1}$. Structural changes occur in the Ru−N bonding framework, which couples low-frequency ν(Ru−N) vibrations to electron transfer. In oxidative electron-transfer quenching, $[Ru(bpy)_3]^{2+*}$, A, $\rightarrow [Ru(bpy)_3]^{3+}$, A^-, an electron is lost from a ligand-based π^*(bpy) level and ν(bpy) vibrations are coupled much as in nonradiative decay.

Both the classical, eq 24, and quantum results, eq 28, show that the vibrational contributions to the barrier decrease as $h\omega$ and ΔQ_e (and S) decrease. ΔQ_e is minimized for couples such as $d\pi^5/d\pi^6$ $[Ru(bpy)_3]^{3+/2+}$ or π^{*0}/π^{*1} $MV^{2+/+}$, where electron transfer involves orbitals that are not involved in the σ-bonding skeleton of the molecule.

IV.B. The Inverted Region. Both the classical and quantum results in eqs 24 and 28 predict that the electron-transfer barrier decreases as $-\Delta G°$ increases. This is only true until $-\Delta G° = \lambda$, at which point classical electron transfer becomes barrierless. As illustrated in Figure 9, the barrier then increases as $-\Delta G°$ is increased further. Figure 9 illustrates the variation in the electron-transfer barrier in the classical limit at fixed λ according to eq 24 for three cases: (A) in the normal region with $-\Delta G° < \lambda$, (B) at the barrierless point, where $-\Delta G° = \lambda$ and $k_{ET} = \nu_{ET}$, and (C) in the inverted region, where $-\Delta G° > \lambda$.

The inverted region was initially predicted by Marcus,[201,208] and the decrease in k_{ET} with $-\Delta G°$ has been observed experimentally many times.[92,209−226] It provides the basis for understanding such phenomena as chemiluminescence and electrochemiluminescence, in which energetic electron transfer gives excited-state products, e.g., $[Ru(bpy)_3]^{3+} + C_2O_4^- \rightarrow [Ru(bpy)_3]^{2+*} + 2CO_2$.[211,227−230]

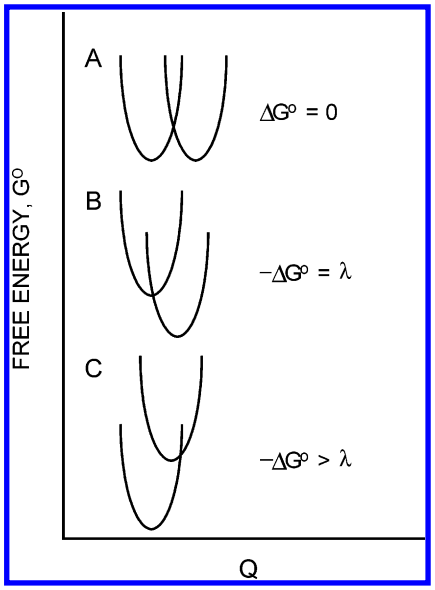

Figure 9. Free energy-coordinate curves illustrating the influence on the classical barrier to electron transfer of increasing $-\Delta G°$ at fixed reorganization energy, λ, according to eq 24. The three cases illustrated are for electron transfer in (A) the normal region with $-\Delta G° < \lambda$, (B) the barrierless point where $-\Delta G° = \lambda$, and (C) the inverted region with $-\Delta G° > \lambda$.

In the normal region, electron transfer occurs by thermal activation and barrier crossing. In the inverted region, excess energy is released in the electron-transfer act. As in nonradiative decay with a coupled high-frequency vibration or vibrations, electron transfer occurs through a series of vibrational channels rather than by a classical barrier crossing. Both quantum and classical barrier crossings are illustrated in Figure 10, with the former illustrating vibrational wave function overlap between the initial and final vibrational wave functions.

(202) Matyushov, D.; Schmid, R. *J. Phys. Chem.* **1994**, *98*, 5152.
(203) Matyushov, D. *Mol. Phys.* **1993**, *79*, 795.
(204) Matyushov, D. *Chem. Phys.* **1993**, *174*, 199.
(205) Basilevsky, M. V.; Rostov, I. V.; Newton, M. D. *Chem. Phys.* **1998**, *232*, 189.
(206) Newton, M. D.; Basilevsky, M. V.; Rostov, I. V. *Chem. Phys.* **1998**, *232*, 201.
(207) Brunschwig, B. S.; Ehrenson, S.; Sutin, N. *J. Phys. Chem.* **1987**, *91*, 4714.
(208) Marcus, R. A. *Discuss. Faraday Soc.* **1960**, *29*, 21.
(209) Miller, J. R.; Beitz, J. V.; Huddleston, R. K. *J. Am. Chem. Soc.* **1984**, *106*, 5057.
(210) Beitz, J. V.; Miller, J. R. *J. Chem. Phys.* **1979**, *71*, 4579.
(211) Wallace, W. L.; Bard, A. J. *J. Phys. Chem.* **1979**, *83*, 1350.
(212) Marcus, R. A. *J. Chem. Phys.* **1965**, *43*, 2654.
(213) Closs, G. L.; Miller, J. R. *Science* **1988**, *240*, 440.
(214) Miller, J. R.; Calcaterra, L. T.; Closs, G. L. *J. Am. Chem. Soc.* **1984**, *106*, 3047.
(215) Closs, G. L.; Calcaterra, L. T.; Green, N. J.; Penfield, K. W.; Miller, J. V. *J. Phys. Chem.* **1986**, *90*, 3673.
(216) Farid, R. S.; Chang, I.-J.; Winkler, J. R.; Gray, H. B. *J. Phys. Chem.* **1994**, *98*, 5176.
(217) Fox, L. S.; Kozik, M.; Winkler, J. R.; Gray, H. B. *Science* **1990**, *247*, 1069.
(218) Wasielewski, M. R.; Niewczyk, M. P.; Svec, W. A.; Pewitt, E. B. *J. Am. Chem. Soc.* **1985**, *107*, 1080.
(219) McLendon, G.; Miller, J. R. *J. Am. Chem. Soc.* **1985**, *107*, 7811.
(220) McLendon, G. *Acc. Chem. Res.* **1988**, *21*, 160.
(221) Ohno, T.; Yoshimura, A.; Mataga, N. *J. Phys. Chem.* **1986**, *90*, 3295.
(222) Gould, I. R.; Ege, D.; Mattes, S. L.; Farid, S. *J. Am. Chem. Soc.* **1987**, *109*, 3794.
(223) Gould, I. R.; Moser, J. E.; Armitage, B.; Farid, S.; Goodman, J. L.; Herman, M. S. *J. Am. Chem. Soc.* **1989**, *111*, 1917.
(224) Chen, P.; Duesing, R.; Tapolsky, G.; Meyer, T. J. *J. Am. Chem. Soc.* **1989**, *111*, 8305.
(225) MacQueen, D. B.; Schanze, K. S. *J. Am. Chem. Soc.* **1991**, *113*, 7470.
(226) Chen, P.; Mecklenburg, S. L.; Duesing, R.; Meyer, T. J. *J. Phys. Chem.* **1993**, *97*, 13126.
(227) Ketter, J. B.; Wightman, R. M. *J. Am. Chem. Soc.* **2004**, *126*, 10183.
(228) Armstrong, N. R.; Wightman, R. M.; Gross, E. M. *Annu. Rev. Phys. Chem.* **2001**, *52*, 391.
(229) Park, S. M.; Bard, A. *J. Phys. Chem. Lett.* **1976**, *38*, 257.
(230) Slaterbeck, A. F.; Meehan, T. D.; Gross, E. M.; Wightman, R. M. *J. Phys. Chem. B* **2002**, *106*, 6088.

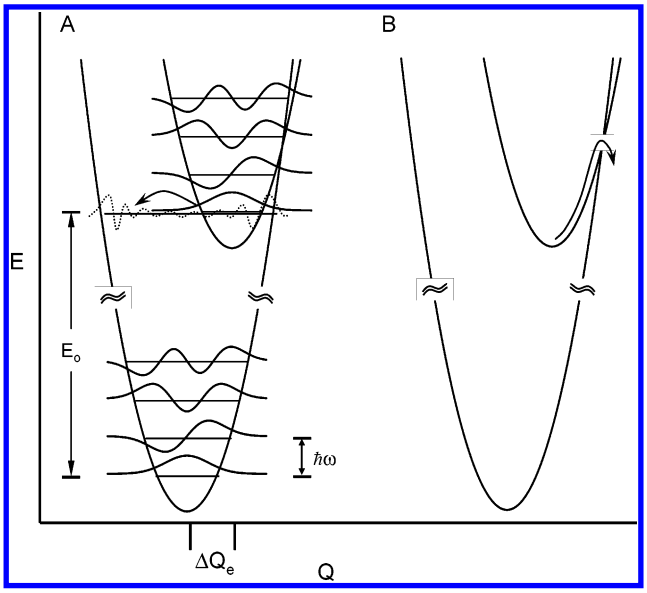

Figure 10. Schematic energy-coordinate ($E-Q$) diagram illustrating electron transfer in the inverted region (A) by a vibrational channel below the intersection region and vibrational wire function overlap between the initial and final vibrational levels (see the text) and (B) by classical barrier crossing.

In the limits $E_o \gg S\hbar\omega$, $\hbar\omega = \hbar\omega'$, and $\hbar\omega \gg k_BT$, the general electron-transfer result in eq 28 takes the energy gap law form in eq 30. It is different from the expression for k_{nr} in eq 20 because it contains H_{DA} rather than V_k and the reorganization energy, $\lambda_{o,L}$, is for electron transfer. The energy gap E_o is related to $\Delta G°$ by $E_o = \Delta G° - \lambda_{o,L}$.[120,130,188,231]

$$k_{ET} = \frac{2\pi}{\hbar}\frac{{H_{DA}}^2}{\sqrt{\hbar\omega E_o}}\exp\left[-S - \frac{\gamma E_o}{\hbar\omega} + \left(\frac{\gamma+1}{\hbar\omega}\right)^2\lambda_{o,L}k_BT\right] \quad (30)$$

$$\gamma = \ln(E_o/S\hbar\omega) - 1 \quad (31)$$

This is a remarkable and important result both for natural and artificial photosynthesis. It predicts that following electron-transfer quenching, e.g., $D-C^*-A \rightarrow D-C^+-A^-$, the rate constant for back electron transfer in the inverted region, $D-C^+-A^- \rightarrow D-C-A$, *becomes slower as the energy stored increases.* Forward electron transfer, $D-C^+-A^- \rightarrow D^+-C-A^-$, is favored at the expense of wasteful back electron transfer, $D-C^+-A^- \rightarrow D-C-A$, which dissipates stored energy as heat.

There are important differences between electron transfer in the normal and inverted regions: (1) In the inverted region, the initial energy-coordinate curve is imbedded in the final curve (Figure 10) and emission can compete with electron transfer.[131,232−239] (2) In the normal region, λ_o contributes to the barrier. In the inverted region, with a coupled high-frequency vibration or vibrations, k_{ET} *increases* as λ_o increases and the solvent's role in energy dissipation is enhanced.[240] (3) In the normal region, electron transfer involves a reordering of the electronic distribution within a single state. In the inverted region, a transition occurs between different, weakly coupled states.

Although they are similar, inverted electron transfer and nonradiative decay are fundamentally different processes. In nonradiative decay, donor−acceptor electronic coupling is strong and the operator in H_{DA} is included in the Hamiltonian defining the two states. They are orthogonal to zero order and mixed by promoting modes [section III.C(ii)]. In inverted electron transfer, electronic coupling mixes the states but is relatively weak, with $H_{DA} < \lambda$.

High-energy electron-transfer products formed after excited-state quenching, e.g., $[Ru(bpy)_3]^{2+}*$, $MV^{2+} \rightarrow [Ru(bpy)_3]^{3+}$, MV^+, for which $-\Delta G° > \lambda$, are called "charge-separated states" or "redox-separated states" (RSSs) to distinguish them from true excited states. In these states, nonradiative decay occurs by electron transfer.

IV.C. Delocalization. Intra-assembly electron transfer in the symbolic molecular assemblies in Figures 1 and 2 occurs through covalent bonds that link the excited state and electron-transfer donors and acceptors. This opens the possibility of significant electronic coupling and delocalization of the transferring electron by orbital mixing. Delocalization decreases the electron-transfer barrier by decreasing structural differences decreasing both ΔQ_e and λ_i. It also decreases the effective electron-transfer distance, which decreases λ_o.[241−246] In the limit of strong electronic coupling, the excess electron is delocalized over both redox sites and there is no structural barrier to electron transfer. Based on a semiclassical analysis by Hush, the localized to delocalized transition occurs when $2H_{DA} \geq \lambda$. This transition can be induced by changes in the ligands and metal so as to enhance electronic coupling. For example, in $[(NH_3)_5Ru^{III}$(4,4′-bipyridine)$Ru^{II}(NH_3)_5]^{5+}$, electronic coupling is weak, 100−200 cm^{-1}, $2H_{DA} \ll \lambda$, and there is a barrier to electron transfer. In $[(NH_3)_5Os^{II.5}$ (pz)$Os^{II.5}(NH_3)_5]^{5+}$ (pz is pyrazine), greater dπ(Os) mixing with the bridging ligand enhances

(231) Brunschwig, B. S.; Sutin, N. *Comments Inorg. Chem.* **1987**, *6*, 209.
(232) Claude, J. P.; Omberg, K. M.; Williams, D. S.; Meyer, T. J. *J. Phys. Chem. A* **2002**, *106*, 7795.
(233) In *Electron Transfer: From Isolated Molecules to Biomolecules, Part One*; Omberg, K. M., Chen, P. Y., Meyer, T. J., Eds.; Wiley & Sons: New York, 1998.
(234) Gould, I. R.; Young, R. H.; Mueller, L. J.; Albrecht, A. C.; Farid, S. *J. Am. Chem. Soc.* **1994**, *116*, 8188.
(235) Gould, S.; Gray, K. H.; Linton, R. W.; Meyer, T. J. *Inorg. Chem.* **1992**, *31*, 5521.
(236) Gould, I. R.; Young, R. H.; Moody, R. E.; Farid, S. *J. Phys. Chem.* **1991**, *95*, 2068.
(237) Gould, I. R.; Young, R. H.; Mueller, L. J.; Albrecht, A. C.; Farid, S. *J. Am. Chem. Soc.* **1994**, *116*, 3147.
(238) Bixon, M.; Jortner, J.; Verhoeven, J. W. *J. Am. Chem. Soc.* **1994**, *116*, 7349.
(239) Gould, I. R.; Farid, S. *Acc. Chem. Res.* **1996**, *29*, 522.
(240) Serron, S. A.; Aldridge, W. S., III; Fleming, C. N.; Danell, R. M.; Baik, M.-H.; Sykora, M.; Dattelbaum, D. M.; Meyer, T. J. *J. Am. Chem. Soc.* **2004**, *126*, 14506.
(241) Demadis, K. D.; Hartshorn, C. M.; Meyer, T. J. *Chem. Rev.* **2001**, *101*, 2655−2685 and references cited therein.
(242) Bublitz, G. U.; Laidlaw, W. M.; Denning, R. G.; Boxer, S. G. *J. Am. Chem. Soc.* **1998**, *120*, 6068.
(243) Hupp, J. T.; Dong, Y.; Blackburn, R. L.; Lu, H. *J. Phys. Chem.* **1993**, *97*, 3278.
(244) Creutz, C.; Newton, M. D.; Sutin, N. *J. Photochem. Photobiol. A* **1994**, *82*, 47.
(245) Reimers, J. R.; Hush, N. S. *J. Am. Chem. Soc.* **1995**, *117*, 1302.
(246) Salaymeh, F.; Berhane, S.; Yusof, R.; de la Rosa, R.; Fung, E. Y.; Matamoros, R.; Lan, K. W.; Zheng, Q.; Kober, E. M.; Curtis, J. C. *Inorg. Chem.* **1993**, *32*, 3895.

Scheme 5. Kinetic Scheme Illustrating the Competing Processes That Occur Following MLCT Excitation of the Anq−$Ru^{II}(b_2m)^{2+}$−PTA D−C−A Assembly Shown in Figure 12[a,254−255]

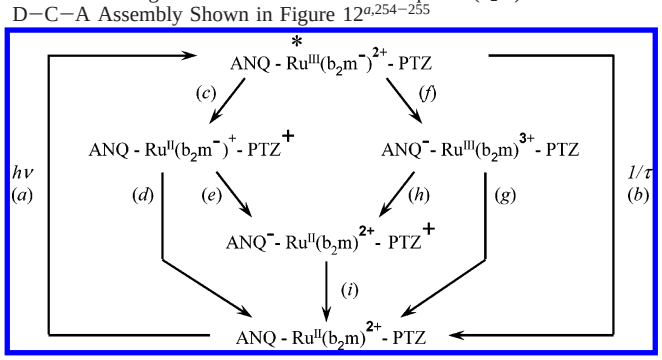

[a] The abbreviations Anq and PTZ are used for the Anq and PTZ derivatives shown in Figure 12.

electronic coupling across the bridge and $2H_{DA} > \lambda$.[241] The effect of electronic coupling on the energy of activation, E_a, in the classical limit is given by eq 32.[176,198,241,247,248]

$$E_a = \frac{\lambda}{4} - |H_{DA}| + \frac{H_{DA}^2}{\lambda} \qquad (32)$$

As H_{DA} approaches λ in magnitude, the Born−Oppenheimer separation of electron and nuclear coordinates, which is assumed in the derivation of eqs 24 and 28, is no longer valid. In their theoretical treatment of this problem, Piepho, Krausz, and Schatz (PKS) define electronic wave functions that are independent of nuclear coordinates and then solve the Schrödinger equation, with the nuclear kinetic energy operator included to give mixed electron−vibrational (vibronic) wave functions, energies, and barriers to electron transfer.[249] The wave functions are expanded in the complete orthonormal set of harmonic oscillator wave functions to give a general solution for the final mixed-coordinate wave functions. The key elements of the PKS model also appear in earlier work including an analysis of electron−phonon coupling in solids by application of linear response theory.[250−253]

IV.E. Kinetic Analysis. The energy conversion scheme in Figure 1 relies on a series of sequential reactions that are kinetically coupled and in competition with others that lead to energy dissipation. The efficiency of formation of the final Redox Separated State (RSS), D^+-C-A^-, assuming $-\Delta G^\circ > \lambda$, depends on the relative magnitudes of the rate constants for a series of competing reactions.

Formation of the RSS. In Scheme 5 is summarized the series of competing reactions that occur upon excitation of a D−C−A array following direct or sensitized excitation. The example used is based on the oligoproline array shown in Figure 12.[34,254,255]

Electron-transfer quenching either reductively, k_c in Scheme 5, or oxidatively, k_f, is in competition with excited-state decay, τ^{-1}. The quenching efficiency is given by $\eta_1 = (k_c + k_f)/(k_c + k_f + \tau^{-1})$. On the basis of the classical result in eq 24, k_c and k_f are dependent on ΔG° and reach maximum values when $-\Delta G^\circ = \lambda$ and the reactions are barrierless.

To put this into perspective, the lifetime of $[Ru(bpy)_3]^{2+*}$ is ~1 μs, depending somewhat on the medium. To achieve $\eta_1 \geq 0.99$ for electron-transfer quenching requires that $k_c + k_f \geq 10^8\ s^{-1}$. With $k_{ET} = 10^{13} \exp\{-[(\Delta G^\circ + \lambda)^2/4\lambda RT]\}$ and $\lambda = 1$ eV, this further requires that $\Delta G^\circ = -0.28$ eV (−6.5 kcal/mol). The maximum rate constant, with $k_c + k_f = 10^{13}\ s^{-1}$, would be reached at $\Delta G^\circ = -1$ eV.

The desire to minimize the electron-transfer barrier by manipulating ΔG° is counterbalanced by the need to maximize the energy available for energy conversion. In the example above, maximizing the quenching rate constant comes at the expense of 1 eV of stored free energy, which could be applied to the fuel-forming reaction.

For the Anq−Ru^{II}(bpy)−PTZ assembly, reductive quenching occurs in the first step to give Anq−Ru^{II}($bpy^{\bullet-}$)−PTZ^+. Subsequent $bpy^{\bullet-} \rightarrow$ Anq electron transfer, k_e in Scheme 5, to give $Anq^{\bullet-}$−Ru^{II}(bpy)−PTZ^+ is in competition with ($bpy^{\bullet-}$) → PTZ^+ back electron transfer to give the ground state k_d. The latter occurs in the inverted region, with k_d decreasing as the ΔG° content of Anq−Ru^{II}($bpy^{\bullet-}$)−PTZ^+ increases. The efficiency of the second electron-transfer step is $\eta_2 = k_e/(k_e + k_d)$. The total efficiency for the formation of the RSS in this case, η_{RSS}, is $\eta_{RSS} = \eta_1\eta_2$.

For the Anq−Ru^{II}(bpy)−PTZ oligoproline assembly, the efficiency of the formation of Anq^-−Ru^{II}(bpy)−PTZ^+ varies from 33 to 86% and the stored redox energy from 1.46 to 1.71 eV depending on the solvent.[254]

Catalyst Activation by Electron Transfer. In Figure 1, the redox equivalents transiently stored in $-D^+-C-A^-$− undergo further electron transfer, from A^- to cat_{red} (k_{red}) and from cat_{ox} to D^+ (k_{ox}). Electron-transfer activation of the catalysts is in competition with back electron transfer between A^- and D^+ (k_{bet}), and the efficiency of catalyst activation, η_{act}, is given by $\eta_{act} = (k_{red} + k_{ox})/(k_{red} + k_{ox} + k_{bet})$. Back electron transfer can occur by long-range electron transfer, $-D^+-C-A^-- \rightarrow -D-C-A-$, or stepwise by reversal of the electron-transfer chains, e.g., $-D^+-C-A^-- \rightarrow -D-C^+-A^-- \rightarrow -D-C-A-$.

In a simplified analysis, the efficiency of $1e^-$ activation of the catalysts, $cat_{ox}-D^+-C-A^--cat_{red} \rightarrow (cat_{ox})^+-D-C-A-(cat_{red})^-$, $\eta_{ET,1}$, is given by $\eta_{ET,1} = \eta_{RSS}(k_{red} + k_{ox})/(k_{red} + k_{ox} + k_{bet}) = \eta_{RSS}\eta_{act}$, with $\eta_{act} = (k_{red} + k_{ox})/(k_{red} + k_{ox} + k_{bet})$.

Assuming that catalyst activation is a $2e^-$ process, there is a final competition between a second light-induced electron transfer to give $(cat_{red})^{2-}$ and $(cat_{ox})^{2+}$, the catalyzed reactions,

(247) Brunschwig, B. S.; Sutin, N. *Coord. Chem. Rev.* **1999**, *187*, 233.
(248) Sutin, N. *Adv. Chem. Phys.* **1999**, *106*, 7.
(249) (a) Reimers, J. R.; Hush, N. S. *Chem. Phys.* **1996**, *208*, 177. (b) Piepho, S. B.; Krausz, E. R.; Schatz, P. N. *J. Am. Chem. Soc.* **1978**, *100*, 2996. (c) Wong, K. Y.; Schatz, P. N. *Prog. Inorg. Chem.* **1981**, *28*, 369. (d) Schatz, P. N. *NATO Adv. Study Inst., Ser. C.* **1980**, *58*. 115.
(250) Fulton, R. L.; Gouterman, M. *J. Phys. Chem.* **1961**, *35*, 5.
(251) Rice, M. J.; Lipari, N. O.; Strassler, S. *Phys. Rev. Lett.* **1977**, *39*, 1359.
(252) Rice, M. J. *Phys. Rev. Lett.* **1976**, *37*.
(253) Rice, M. J.; Yartsev, V. M.; Jacobsen, C. S. *Phys. Rev. B* **1980**, *21*, 3437.
(254) Striplin, D. R.; McCafferty, D. G.; Wall, C. G.; Friesen, D. A.; Erickson, B. W.; Meyer, T. J. *J. Am. Chem. Soc.* **2004**, *126*, 5282.
(255) Slate, C. A.; Striplin, D. R.; Moss, J. A.; Chen, P. Y.; Erickson, B. W.; Meyer, T. J. *J. Am. Chem. Soc.* **1998**, *120*, 4885.

Scheme 6

	E^o, V vs NHE
$2\ H_2O \rightarrow O_2 + 4\ H^+ + 4\ e^-$	1.23
$H_2O \rightarrow\ ^{\cdot}OH + H^+ + e^-$	2.10
$CO_2 + 2\ e^- + 2H^+ \rightarrow HCOOH$	-0.22
$CO_2 + e^- \rightarrow CO_2^{\cdot-}$	-1.9
$CO_2 + 2\ e^- \rightarrow CO_2^{2-}$	-1.45

$k_{cat,red}$ and $k_{cat,ox}$, and $(cat_{red})^- \rightarrow (cat_{ox})^+$ back electron transfer. Even with well-separated catalysts, back-electron-transfer "leakage" through the assembly can have a deleterious effect on the fuel-forming reaction.

More complex catalytic activation schemes, such as the $4e^-$ oxidation of water, add additional competitive steps that can contribute deleteriously to the overall efficiency.

Based on an analysis by Sergei Lymar of Brookhaven National Laboratory, the minimum rate requirement for efficient activation and reactivity of the catalysts can be estimated based on the AM 1.5 solar irradiance spectrum, with AM 1.5 the accepted spectral standard for sunlight at an angle of incidence of 45°. For the solar spectrum at $\lambda <$ 600 nm, the incident irradiance is $\sim$30 mW cm^{-2} or approximately 1.3×10^{-7} einsteins $cm^{-2}\ s^{-1}$ (assuming 500-nm photons). With a 100% redox separation efficiency and a catalyst coverage density of 1 nm^{-2}, a system turnover rate, including the catalyst reactions, of $\sim 10^2\ s^{-1}$ is needed to ensure that solar irradiance is rate limiting. This means that each step in the excitation/electron transfer/catalyst activation/fuel generating cycle must occur with $\tau < 10$ ms. As a useful reference, the individual activation steps in the photochemical oxidation of H_2O by photosystem II occur on the microsecond to submillisecond time scale with up to 50 molecules of O_2 produced per second; see below.

V. Electron-Transfer Activation of Catalysis

V.A. Catalyst Activation. Proton-Coupled Electron Transfer (PCET). Gain or loss of multiple electrons is required to activate the fuel-forming catalysts and avoid high-energy $1e^-$ intermediates such as $CO_2^{\bullet-}$ or $^{\bullet}OH$. Their impact energetically can be seen by comparing $E^{\circ\prime}$ values in Scheme 6. The $2e^-$ entry for CO_2 to CO_2^{2-} illustrates the deleterious effect of an intermediate that is at high energy in proton content.

The need for multielectron change necessitates complex pathways and the transfer of more than one electron to or from the catalysts. Charge compensation is required to avoid large increases in stepwise redox potentials in order to achieve redox potential leveling. This is especially important for biological redox couples in nonpolar membrane environments, where charge compensation by the surrounding dielectric is low compared to water, for example. Charge compensation can occur by ion pairing, extrusion, or addition of ions from chemical bonds and, most importantly, by PCET.

The influence of PCET can be seen by the decrease of over 1 V for the $2e^-$ reduction of CO_2 to HCO_2H compared to CO_2^{2-} in Scheme 6. PCET is a natural consequence of the effect of electron content on acid−base properties. For example, oxidation of $[Fe(H_2O)_6]^{2+}$ to $[Fe(H_2O)_6]^{3+}$ decreases $pK_{a,1}$ from 9.5 to 2.2[256] and oxidation of tyrosine (TyrOH) to its cation radical, $TyrOH^{\bullet+}$, decreases the pK_a from +10 to −2.[257−260] Both of these couples are pH-dependent over a wide pH range, with the $TyrOH^{\bullet+}$/TyrOH couple decreasing by 0.59 mV/pH unit from below pH = 0 to 0.94 V at pH = 7.

The electrostatic effect of PCET can dramatically decrease sequential redox potentials, making the buildup of multiple reductive or oxidative equivalents by electron transfer feasible over a relatively small potential range. As an illustration, $\Delta E^{\circ\prime}$ between the $Ru^{IV/III}$/*cis*-$[Ru(bpy)_2Cl_2]^{2+/+}$ and $Ru^{III/II}$/*cis*-$[Ru(bpy)_2Cl_2]^{2+}$ couples in CH_3CN is 1.7 V. It is only 0.11 V between the [*cis*-$Ru^{IV}(bpy)_2(py)(O)]^{2+}$/[*cis*-$Ru^{III}(bpy)_2(py)(OH)]^{2+}$ and [*cis*-$Ru^{III}(bpy)_2(py)(OH)]^{2+}$/[*cis*-$Ru^{II}(bpy)_2(py)(H_2O)]^{2+}$ couples in water.[261−263]

There is a happy coincidence in this. Both protons and electrons are involved in the fuel-forming half-reactions in eqs 1−3, e.g., $2H_2O \rightarrow O_2 + 4e^- + 4H^+$, and activation of key redox steps also requires PCET, e.g.,

$$M{-}OH_2^{n+} \xrightarrow{-2e^-/2H^+} M{=}O^{264}$$

In this case, PCET both levels the redox potentials and activates the catalyst for subsequent reaction.[264]

V.B. Electron−Proton Transfer (EPT). In catalyst activation by PCET, the gain or loss of protons can be rate-limiting. An example is the oxidation of *cis*-$[Ru^{III}(bpy)_2(py)(OH)]^{2+}$ to catalytically active *cis*-$[Ru^{IV}(bpy)_2(py)(O)]^{2+}$, in which loss of a proton is rate-limiting, followed by rapid electron transfer.[265] This reaction could occur by electron transfer, followed by proton transfer, but with an energy penalty because $E^{\circ\prime} > 1.6$ V (vs NHE) for the *cis*-$[Ru^{IV}(bpy)_2(py)(OH)]^{3+}$/*cis*-$[Ru^{III}(bpy)_2(py)(OH)]^{2+}$ couple. There is also an energy penalty for the pathway involving proton transfer to give *cis*-$[Ru^{III}(bpy)_2(py)(O)]^+$ followed by electron transfer. For $Ru^{III}{-}OH^{2+}$, $pK_a > 13$, and loss of a proton at pH = 7 is endoergic by $\Delta G^{\circ} > +0.42$ eV (>+9.7 kcal/mol).[265]

As shown in the $E^{\circ\prime}$ diagram at pH = 7 in Scheme 7, the energy-efficient pathway for interconverting *cis*-$[Ru^{III}(bpy)_2(py)(OH)]^{2+}$ and *cis*-$[Ru^{IV}(bpy)_2(py)(O)]^{2+}$ is by coupled loss

(256) Baes, C. F., Jr.; Messmer, R. E. *The Hydrolysis of Metal Cations*; R. E. Krieger Publishing Co.: Malabar, FL, 1986.
(257) Sjödin, M.; Styring, S.; Akermark, B.; Sun, L.; Hammarström, L. *J. Am. Chem. Soc.* **2000**, *122*, 3932.
(258) Hammarström, L. *Curr. Opin. Chem. Biol.* **2003**, *7*, 666.
(259) Sjodin, M.; Styring, S.; Wolpher, H.; Xu, Y.-H.; Sun, L. C.; Hammarstrom, L. *J. Am. Chem. Soc.* **2005**, *127*, 3855.
(260) Sun, L. C.; Hammarström, L.; Akermark, B.; Styring, S. *Chem. Soc. Rev.* **2001**, *30*, 36.
(261) Moyer, B. A.; Meyer, T. J. *J. Am. Chem. Soc.* **1978**, *100*, 3601.
(262) Moyer, B. A.; Meyer, T. J. *Inorg. Chem.* **1981**, *20*, 436.
(263) Binstead, R. A.; Moyer, B. A.; Samuels, G. J.; Meyer, T. J. *J. Am. Chem. Soc.* **1981**, *103*, 2897.
(264) Meyer, T. J.; Huynh, M. V. H. *Chem. Rev.* **2005**, in preparation.
(265) Lebeau, E. L.; Binstead, R. A.; Meyer, T. J. *J. Am. Chem. Soc.* **2001**, *23*, 10535.

Scheme 7. PCET Thermodynamics for the Couples *cis*-$[Ru^{IV}(bpy)_2(py)(O)]^{2+}$/*cis*-$[Ru^{III}(bpy)_2(py)(OH)]^{2+}$ and *cis*-$[Ru^{III}(bpy)_2(py)(OH)]^{2+}$/*cis*-$[Ru^{II}(bpy)_2(py)(H_2O)]^{2+}$ Illustrating the Energy Advantage of a Coupled EPT Pathway

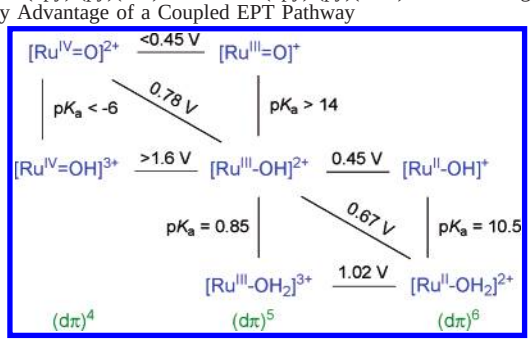

of electrons and protons (EPT) to give *cis*-$[Ru^{IV}(bpy)_2(py)(O)]^{2+}$ directly. $E^{\circ\prime}$ for this half-reaction at pH = 7 is only 0.78 V.

Although advantageous energetically, the mechanistic details for a EPT pathway are necessarily more complex than either electron or proton transfer because both electrons and protons are transferred simultaneously. This means, for example, that both the electron donor and acceptor must have available orbitals for undergoing coupled EPT.[264]

EPT is the pathway used in the comproportionation reaction between *cis*-$[Ru^{IV}(bpy)_2(py)(O)]^{2+}$ and *cis*-$[Ru^{II}(bpy)_2(py)(H_2O)]^{2+}$ shown in eq 33. A tip-off that EPT is operative is the fact that the reaction occurs with $k(H_2O)/k(D_2O) = 16$. The EPT pathway is illustrated in eq 34. It features electron transfer from a dπ(Ru^{II}) orbital to a dπ-(Ru^{IV}) orbital and proton transfer from σ_{O-H} to a lone pair on the oxo group.

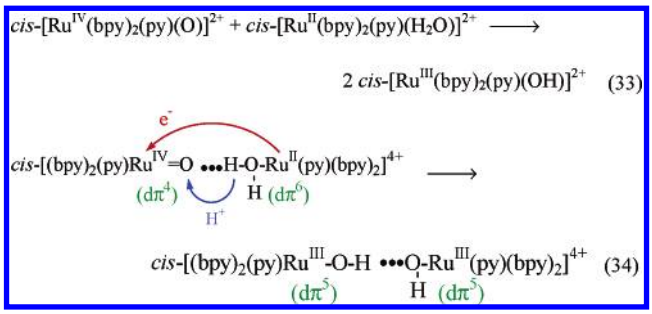

PCET and EPT play major roles in biology, in respiration and photosynthesis, for example. As noted in section III.A and Figure 5, in photosystem II D → C* → A electron transfer from tyrosine Y_Z to Q_A, initiated by oxidative quenching of P_{680}* by an adjacent phenophytin, triggers water oxidation. It has been suggested that electron transfer from Y_Z is coupled to proton transfer to H-bonded histidine, His-190 (Scheme 8).[266−271]

Scheme 8. Comparative Energetics of Oxidation of Tyrosine Y_Z by Electron Transfer and by MS-EPT

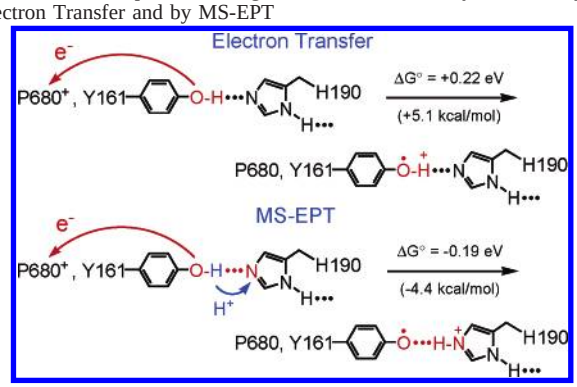

Because electron and proton transfer involve different electron and proton acceptors, this pathway is called multiple site EPT, or MS-EPT. From the comparative energetics in Scheme 8, MS-EPT offers an energy advantage over electron transfer of 9.5 kcal/mol in the oxidation of Y_Z because it avoids the high-energy radical cation intermediate, $TyrOH^{+\bullet}$.

The theory of EPT has been developed by Cukier and Hammes-Schiffer and their co-workers based on somewhat different assumptions.[272−287] Both are based on electron-transfer theory and include proton transfer as a coupled high- or medium-frequency mode, ν(E−H). In the treatment by Hammes-Schiffer et al., strong electronic coupling between the intial and final proton-transfer states is assumed, giving rise to new adiabatic proton-coupled states. Electronic coupling between the resulting proton adiabatic states is treated subsequently as in electron-transfer theory; see section IV.

Application of the time-dependent perturbation theory with application of the Golden Rule to the transition between the final proton- and electron-coupled states I and II leads to the expression for coupled EPT in eq 35a for D−H- - -A → D- - -H−A EPT.[274]

As in eq 28 for electron transfer, the summations are over a series of vibrational channels, in this case from the initial, coupled D−H- -A vibrational levels μ to the final coupled D- - -H−A levels ν. In contrast to eq 28, levels above $\mu = 0$ are included in the summations. $P_{l\mu}$ is the Boltzmann population in vibrational level μ in the initial state,

(266) Tommos, C.; Babcock, G. T. *Acc. Chem. Res.* **1998**, *31*, 18.
(267) Hoganson, C. W.; Babcock, G. T. *Science* **1997**, *277*, 1953.
(268) Remy, A.; Gerwert, K. *Nat. Struct. Biol.* **2003**, *10*, 637.
(269) Proshlyakov, D. A.; Pressler, M. A.; Babcock, G. T. *Proc. Natl. Acad. Sci. U.S.A.* **1998**, *95*, 8020 and references cited therein.
(270) Babcock, G. T.; Espe, M.; Hoganson, C.; LydakisSimantiris, N.; McCracken, J.; Shi, W. J.; Styring, S.; Tommos, C.; Warncke, K. *Acta Chim. Scand.* **1997**, *51*, 533.
(271) Hoganson, C. W.; Lydakis Simantiris, N.; Tang, X. S.; Tommos, C.; Warncke, K.; Babcock, G. T.; Diner, B. A.; McCracken, J.; Styring, S. *Photosynth. Res.* **1995**, *46*, 177.
(272) Cukier, R. I.; Nocera, D. G. *Annu. Rev. Phys. Chem.* **1998**, *49*, 337.
(273) Soudackov, A.; Hammes-Schiffer, S. *J. Chem. Phys.* **1999**, *111*, 4672.
(274) Soudackov, A.; Hammes-Schiffer, S. *J. Chem. Phys.* **2000**, *113*, 2385.
(275) Soudackov, A.; Hatcher, E.; Hammes-Schiffer, S. *J. Chem. Phys.* **2005**, *122*, 014505/1.
(276) Hammes-Schiffer, S. *Acc. Chem. Res.* **2001**, *34*, 273.
(277) Decornez, H.; Hammes-Schiffer, S. *J. Phys. Chem. A* **2000**, *104*, 9370.
(278) Rostov, I.; Hammes-Schiffer, S. *J. Chem. Phys.* **2001**, *115*, 285.
(279) Hammes-Schiffer, S.; Iordanova, N. *Biochim. Biophys. Acta* **2004**, *1655*, 29.
(280) Shin, S.; Cho, S.-I. *Chem. Phys.* **2000**, *259*, 27.
(281) Iordanova, N.; Decornez, H.; Hammes-Schiffer, S. *J. Am. Chem. Soc.* **2001**, *123*, 3723.
(282) Iordanova, N.; Hammes-Schiffer, S. *J. Am. Chem. Soc.* **2002**, *124*, 4848.
(283) Hammes-Schiffer, S. *Electron Transfer in Chemistry: Principles, Theories, Methods, and Techniques*; Wiley-VCH: Weinheim, Germany, 2001.
(284) Hammes-Schiffer, S. *ChemPhysChem* **2002**, *3*, 33.
(285) Cukier, R. I. *J. Phys. Chem.* **1994**, *98*, 2377.
(286) Cukier, R. I. *J. Phys. Chem.* **1996**, *100*, 15428.
(287) Cukier, R. I. *J. Phys. Chem. B* **2002**, *106*, 1746.

D−H- - -A. $\lambda_{\mu\nu}$ is the reorganization energy arising from the solvent and low-frequency modes for the $\mu \rightarrow \nu$ vibrational channel, and $\Delta G_{\mu\nu}°$ is the free-energy change for the $\mu \rightarrow \nu$ channel (eq 35b).[279,284]

The expression for k_{EPT} in eq 35a has been extended to include coupled high-frequency vibrations treated quantum mechanically and anharmonic modes such as ν_{O-H} coupled in the proton-transfer coordinate.[274,281]

$$k_{EPT} = \frac{2\pi}{\hbar\sqrt{4\pi\lambda_{\mu\nu}k_B T}} \sum_{\mu} P_{I\mu} \sum_{\nu} |V_{\mu\nu}|^2 \exp\left\{-\left[\frac{(\Delta G_{\mu\nu}° + \lambda_{\mu\nu})^2}{4\lambda_{\mu\nu}k_B T}\right]\right\} \quad (35a)$$

$$\Delta G_{\mu\nu}° = \Delta G° + (\mu - \nu)h\nu \quad (35b)$$

The reorganization energies, free-energy change, and couplings in eq 35a are different for each vibrational channel because of slight differences in the proton-transfer distance. The summation over μ typically involves a limited number of levels ($\leq$4); those for which $-\Delta G_{\mu\nu}°$ is not greatly different from $\lambda_{\mu\nu}$ to minimize the classical exponential barrier term.

$V_{\mu\nu}$ is the EPT matrix element for the $\mu \rightarrow \nu$ vibrational channel. If the Condon approximation separating nuclear and electronic motion is valid, it is given by eq 36a, in which $V_{ET} = H_{DA}$, the electron-transfer matrix element in eq 25. In this limit, the frequency factor for EPT barrier crossing, ν_{EPT}, is given by eq 36b.

$$V_{\mu\nu} \approx V_{ET}\langle\phi_\mu^{I}|\phi_\nu^{II}\rangle \quad (36a)$$

$$\nu_{EPT}(\mu \rightarrow \nu) = \frac{2\pi}{\hbar\sqrt{4\pi\lambda_{\mu\nu}k_B T}} V_{ET}^2\langle\phi_\mu^{I}|\phi_\nu^{II}\rangle^2 \quad (36b)$$

In eq 36, ϕ_μ^{I} and ϕ_ν^{II} are proton vibrational wave functions for the adiabatic, mixed initial and final proton states. As for electron transfer and participation by high- or medium-frequency modes (eq 28), the square of the overlap integral, $\langle\phi_\mu^{I}|\phi_\nu^{II}\rangle^2$, gives a quantitative measure of the extent to which the reactants and products coexist spatially, in this case along the proton-transfer coordinate. Site-to-site transfer distances for proton transfer and EPT are large compared, for example, to changes in equilibrium displacements for coupled vibrations for electron transfer. Consequently, the vibrational integrals for proton transfer are small. This makes $V_{ET}\langle\phi_\mu|\phi_\mu\rangle$ in eq 36a small, justifying the assumption that EPT is nonadiabatic, with ν_{ET} varying as the square of V_{ET} as in eq 36b even if electronic coupling is significant.

In general, $V_{\mu\nu}$, is a function of the coordinates of both the transferring electron and proton. Procedures are available for solving the Schrödinger equation in this limit, giving wave functions and energies that are functions of both electronic and nuclear coordinates, as described for the PKS theory in section IV.C.

The theories for EPT developed by Cukier and Hammes-Schiffer have proven especially useful in understanding relative rate constants, solvent effects, kinetic isotope effects, etc.[272−283,285−287]

Scheme 9. Reaction Sequence in the Oxidation of Water by *cis,cis*-$[(bpy)_2(H_2O)Ru^{III}ORu^{III}(H_2O)(bpy)_2]^{4+}$ Showing Stepwise PCET Oxidation to $[(bpy)_2(O)Ru^{V}(ORu^{V}(O)(bpy)_2]^{4+}$ Followed by Water Oxidation[289,296]

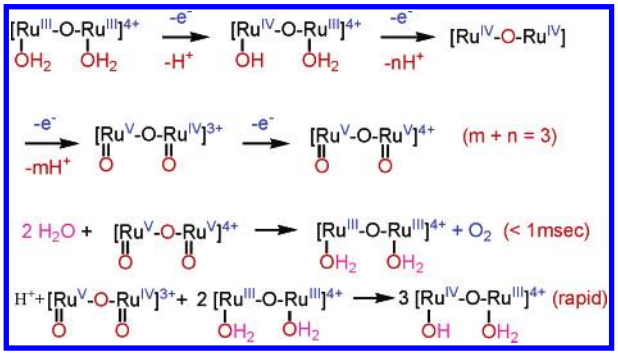

VI. Catalytic Reactions

The greatest chemical challenge in the modular approach to artificial photosynthesis is identifying catalysts that have the ability to carry out the necessary multiple electron transformations at energies and rates consistent with the solar irradiance. Based on the accessibility of pathways such as atom transfer, hydride transfer, oxidative addition, reductive elimination, insertion, etc., catalysts must be identified with the reactivities required to carry out the small-molecule transformations of artificial photosynthesis. The required characteristics include (1) activation by sequential 1e$^-$ transfers and, where needed energetically, the availability of EPT pathways, (2) redox potentials sufficient to drive the half-reactions, (3) reaction rates for catalyst turnover that are sufficiently rapid that solar irradiance is rate-limiting, and (4) strategies for incorporating modules and components into assemblies and assemblies into devices.

Oxo Complexes and Water Oxidation. As shown in Scheme 7, 2e$^-$/2H$^+$ oxidation of *cis*-$[Ru^{II}(bpy)_2(py)(H_2O)]^{2+}$ gives *cis*-$[Ru^{IV}(bpy)_2(py)(O)]^{2+}$, which is an active oxidation catalyst. It utilizes a variety of pathways for oxidizing organics and inorganics including O-atom transfer/epoxidation, H-atom and hydride transfer, EPT, and C−H bond insertion.[288] It becomes a catalyst for water oxidation when linked to a second Ru in *cis,cis*-$[(bpy)_2(H_2O)Ru^{III}ORu^{III}(H_2O)(bpy)_2]^{4+}$ (Scheme 9).[289−297]

Activation of the catalyst occurs by chemical or electrochemical oxidation with PCET 4e$^-$/4H$^+$ loss over a range of only 0.4 V at pH = 1 to give the active form of the

(288) Meyer, T. J.; Huynh, M. V. H. *Inorg. Chem.* **2003**, *42*, 8140.
(289) Binstead, R. A.; Chronister, C. W.; Ni, J.; Hartshorn, C. M.; Meyer, T. J. *J. Am. Chem. Soc.* **2000**, *122*, 8464.
(290) Raven, S. R.; Meyer, T. J. *Inorg. Chem.* **1988**, *27*, 4478.
(291) Yagi, M.; Kaneko, M. *Chem. Rev.* **2001**, *101*, 21.
(292) Geselowitz, D.; Meyer, T. J. *Inorg. Chem.* **1990**, *29*, 3894.
(293) Hurst, J. K. *Coord. Chem. Rev.* **2005**, *249*, 313.
(294) Yamada, H.; Siems, W. F.; Koike, T.; Hurst, J. K. *J. Am. Chem. Soc.* **2004**, *126*, 9786.
(295) Yang, X.; Baik, M.-H. *J. Am. Chem. Soc.* **2004**, *126*, 13222.
(296) Gilbert, J. A.; Eggleston, D. S.; Murphy, W. R.; Geselowitz, D. A.; Gersten, S. W.; Hodgson, D. J.; Meyer, T. J. *J. Am. Chem. Soc.* **1985**, *107*, 3855.
(297) Sens, C.; Romero, I.; Rodriguez, M.; Llobet, A.; Parella, T.; Benet-Buchholz, J. *J. Am. Chem. Soc.* **2004**, *126*, 7798.

catalyst, $[(bpy)_2(O)Ru^{V}ORu^{V}(O)(bpy)_2]^{4+}$. As shown by electrochemical measurements and oxidation by Ce(IV), oxidative activation involves a sequence of sequential $1e^-$ steps, e.g.,

$$[(H_2O)Ru^{III}-O-Ru^{III}(H_2O)]^{4+} \xrightarrow{-e^-/H^+} [(OH)Ru^{IV}-O-Ru^{III}(H_2O)]^{4+}$$

with the intermediate $Ru^{IV}-O-Ru^{IV}$ unstable with respect to disproportionation, Scheme 9.

Following the water oxidation step, a rapid cross reaction occurs between the lower and higher oxidation state forms $Ru^{III}-O-Ru^{III}$ and $Ru^{V}-O-Ru^{IV}$ to give $[(OH)Ru^{IV}-O-Ru^{III}(H_2O)]^{4+}$ as the final product of a single cycle as shown by stopped-flow measurements with Ce(IV) as the oxidant.[289,296] The stopped-flow measurements also reveal that, once formed, $[(bpy)_2(O)Ru^{V}ORu^{V}(O)(bpy)_2]^{4+}$ oxidizes H_2O to O_2 on the submillisecond time scale.[289]

With Ce(IV) as the oxidant in acidic solution, the overall catalytic reaction is shown in eq 37. The catalytic chemistry is complicated by anation and formation of $[(bpy)_2(X)Ru^{IV}ORu^{III}(OH_2)(bpy)_2]^{4+}$ ($X = ClO_4$, CF_3SO_3) after only a few catalytic turnovers. The catalyst retains its ability to oxidize H_2O to O_2 but only after aquation occurs to give back $[(bpy)_2(OH)Ru^{IV}ORu^{III}(OH_2)(bpy)_2]^{4+}$. Reasonable mechanisms have been proposed for the O_2 evolution step based on kinetic and ^{18}O-labeling measurements, but the actual pathway or pathways that dominate are unclear because of ambiguities in interpreting the data.[289]

$$4Ce(IV) + 2H_2O \xrightarrow{[(bpy)_2(H_2O)RuORu(H_2O)(bpy)_2]^{4+}} 4Ce(III) + O_2 + 4H^+ \quad (37)$$

The most recent, 3.5-Å resolution, structure of photosytem II shows that the oxygen-evolving complex (OEC) consists of an oxo-bridged Mn_3Ca cluster with an appended Mn site linked by a μ-oxo bridge.[24,299] On the basis of the structure of the core and the surrounding EPT apparatus, it appears that the appended Mn may be a site for oxidative cycling between Mn^{II} and Mn^{V}. The suggestion has been made that the key O- - -O bond-forming step may involve intermediate $Mn^{III}-OOH$ formation by attack of OH^- coordinated to Ca on the oxyl O atom (eq 38).[24,299,300]

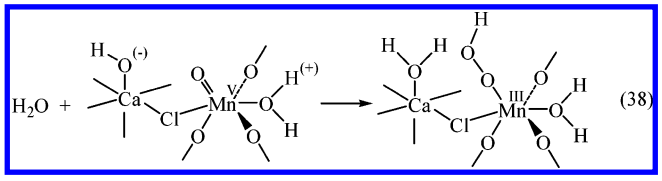

CO_2 Reduction. There is an extensive coordination and reactivity chemistry of CO_2 with transition-metal complexes.[7,301−305] This includes both electrochemical and photochemically driven reduction to give as typical products CO, HCO_2^-, and $C_2O_4^{2-}$.[7,301,305−309] Polypyridyl complexes such as $[M(bpy)_2(CO)H]^+$ (M = Os,Ru) and $Re(bpy)(CO)_3Br$, metal porphyrins, and metal macrocyclic complexes have all proven to be effective catalysts once they undergo reduction at metal or ligand-based orbitals.

Two of the key CO_2 activation pathways that have been identified or invoked are (1) CO_2 insertion as in *fac*-(bpy)-$(CO)_3Re-H + CO_2 \rightarrow$ *fac*-(bpy)$(CO)_3Re-OC(O)H$ and (2) metallocarboxylic acid formation as in $Co^{I}(HMD)^+ + CO_2 + S \rightarrow [S-Co^{III}(HMD)(CO_2^{2-})]^+$ (HMD = 5,7,7,12,14,14-hexamethyl-1,4,8,11-tetraazacyclotetradeca-4,11-diene). In the latter case, protonation, $[S-Co^{III}(HMD)(CO_2^{2-})]^+ + HA \rightarrow [S-Co^{III}(HMD)(CO_2H)]^{2+} + A$, followed by reduction, $[S-Co^{III}(HMD)(CO_2H)]^{2+} + e^- \rightarrow [Co^{II}(HMD)]^{2+} + CO + OH^- + S$, releases CO as the CO_2 reduction product.[301] In the former case, reduction of the formate complex in the presence of a proton source releases formate anion ($HCOO^-$), regenerating the hydride.[309,310]

One advantage of the modular approach to artificial photosynthesis is that catalysts as potential modules can be screened toward electron-transfer activation by simple electrochemical measurements and appended later into multifunctional molecular assemblies.

VII. Assembly Strategies

A strategy is required to organize reactive modules into multifunctional assemblies. This places significant demands on the underlying synthetic chemistry, which must provide (1) accessibility to a range of active modules, (2) a sequential addition strategy that allows for control of both sequence and spatial order, (3) a linkage chemistry compatible with the surrounding environment and the reactive forms of the catalysts, (4) general stability as a unit, and (5) the ability to be scaled up synthetically.

Three different strategies have been explored for the preparation of multifunctional assemblies based on polypyridyl complexes.

Sequential Covalent Bond Formation. Elegant assemblies have been constructed from derivatized porphyrins and organics.[2−6] Related strategies have been developed for polypyridyl complexes based on sequential covalent bond formation through linkages either between metals or between ligands.[54,58,59,65−73] The assembly in Figure 4 illustrates an

(298) Hupp, J. T.; Otruba, J. P.; Parus, S. J.; Meyer, T. J. *J. Electroanal. Chem.* **1985**, *190*, 287.
(299) McEvoy, J. P.; Brudvig, G. W. *Phys. Chem. Chem. Phys.* **2004**, *6*, 4754.
(300) Meyer, T. J.; Huynh, M. V. H.; Thorp, H. H., in preparation.
(301) Fujita, E. *Coord. Chem. Rev.* **1999**, *185−186*, 373.
(302) Gibson, D. H. *Chem. Rev.* **1996**, *96*, 2063.
(303) Gibson, D. H. *Coord. Chem. Rev.* **1999**, *185−186*, 335.
(304) Jessop, P. G.; Ikariya, T.; Noyori, R. *Chem. Rev.* **1995**, *95*, 259.
(305) Meyer T. J. *Carbon Dioxide Fixation and Reduction in Biological and Model Systems*; Oxford University Press: Oxford, U.K., 1994; Chapter 14, pp 211−224.
(306) Lehn, J.-M.; Ziessel, R. *J. Organomet. Chem.* **1990**, *382*, 157.
(307) Ishida, H.; Terada, T.; Tanaka, K.; Tanaka, T. *Inorg. Chem.* **1990**, *29*, 905.
(308) Sullivan, B. P.; Bruce, M. R. M.; O'Toole, T. R.; Bolinger, C. M.; Megehee, E.; Thorp, H.; Meyer, T. J. *Electrocatalytic Carbon Dioxide Reduction*; American Chemical Society: Washington, DC, 1988; Vol. 363, Chapter 6, pp 52−90.
(309) Sutin, N.; Creutz, C.; Fujita, E. *Comments Inorg. Chem.* **1997**, *19*, 67.
(310) Pugh, J. R.; Bruce, M. R. M.; Sullivan, B. P.; Meyer, T. J. *Inorg. Chem.* **1991**, *30*, 86.

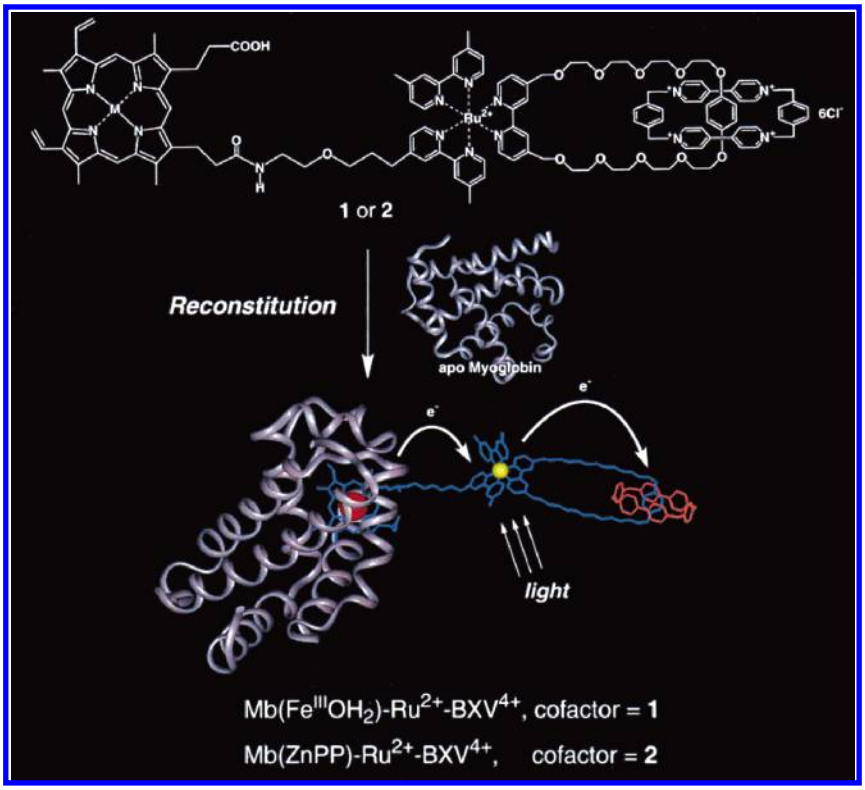

Figure 11. Illustration of the structures of two triad molecular assemblies including one that contains apomyoglobin linked to a Ru(bpy) chromophore and a catenane-type pyridinium electron acceptor. Reconstitution of the derivatized myoglobin and excitation are followed by oxidative electron transfer and oxidation of $Fe^{III}-OH_2$.[314]

example of the latter. There has also been significant progress in creating assemblies in which a Ru(bpy) chromophore is coupled to a potentially reactive catalyst site. Notable in this regard is a series of Ru(bpy) derivatives incorporating both tyrosine and appended Mn dimers as models for the key activation steps that occur in photosystem II.[257−260,311−313]

Another is the linked assembly shown in Figure 11 from the elegant work of Hamachi et al., in which an apomyoglobin (cofactor = 1) was chemically linked to a Ru(bpy) derivative and to a catenane-type pyridinium acceptor. Reconstitution of the myoglobin and visible excitation led to oxidation of the $Fe^{III}-OH_2$ site in the modified myoglobin.[314,315]

An early example of the ligand-bridging strategy was the mixed-valence complex $[(dpte)_2ClRu^{II}(4,4'\text{-bipyridine})Ru^{III}Cl(bpy)_2]^{3+}$ (dpte is $PhSCH_2CH_2SPh$) in which $Ru^{II} \rightarrow (4,4'\text{-bipy})$ excitation leads to $4,4'\text{-bipy}^{\bullet-} \rightarrow$ bpy electron transfer across the bridge and $[(dpte)_2ClRu^{III}(4,4'\text{-bipyridine})Ru^{III}Cl(bpy^{\bullet-})(bpy)]^{3+*}$ as a photochemical transient.[316,317] Some highly evolved and intricate examples have come from stepwise reactions and dendrimer formation. This includes a series of ligand-bridged dendrimers based on ruthenium polypyridyl complexes. The photophysics of the resulting assemblies have been investigated in detail.[318−320]

There are significant limitations in the preparation of molecular assemblies by sequential covalent bond formation. This approach necessarily involves a stepwise sequence of reactions with penalties for yields of less than 100% at each step, which can greatly diminish overall yields in multistep syntheses.

Derivatization of Preformed Polymers. An alternate strategy involves the derivatization of preformed polymers.[34,94,321−331]

(311) Magnuson, A.; Berglund, H.; Korall, P.; Hamarström, L.; Akermark, B.; Styring, S.; Sun, L. C. *J. Am. Chem. Soc.* **1997**, *119*, 10720.
(312) Sjödin, M.; Ghanem, R.; Polivka, T.; Pan, J.; Styring, S.; Sun, L. C.; Sundström, V.; Hammarström, L. *Phys. Chem. Chem. Phys.* **2004**, *6*, 4851.
(313) Carra, C.; Iordanova, N.; Hammes-Schiffer, S. J. *J. Am. Chem. Soc.* **2003**, *125*, 10429.
(314) Hu, Y.-Z.; Tsukiji, S.; Shinkai, S.; Oishi, S.; Hamachi, I. *J. Am. Chem. Soc.* **2000**, *122*, 241.
(315) Hamachi, I.; Tsukiji, S.; Shinkai, S.; Oishi, S. *J. Am. Chem. Soc.* **1999**, *121*, 5500.
(316) Schanze, K. S.; Meyer, T. J. *Inorg. Chem.* **1985**, *24*, 2121.
(317) Curtis, J. C.; Bernstein, J. S.; Meyer, T. J. *Inorg. Chem.* **1985**, *24*, 385.
(318) Constable, E. C. *Chem. Commun.* **1997**, 1073.
(319) Balzani, V.; Ceroni, P.; Juris, M.; Venturi, M.; Campagna, S.; Puntotiero, F.; Serroni, S. *Coord. Chem. Rev.* **2001**, *219*, 545.
(320) Balzani, V.; Campagna, S.; Denti, G.; Juris, A.; Serroni, S.; Venturi, M. *Acc. Chem. Res.* **1998**, *31*, 26.
(321) Galoppini, E.; Fox, M. A. *J. Am. Chem. Soc.* **1996**, *118*, 2299.
(322) Clements, J. H.; Webber, S. E. *J. Phys. Chem. B* **1999**, *103*, 9366.
(323) Clements, J. H.; Webber, S. E. *J. Phys. Chem. A* **1999**, *103*, 2513.
(324) Schillén, K.; Yekta, A.; Ni, S.; Farinha, J. P. S.; Winnik, M. A. *J. Phys. Chem. B* **1999**, *103*, 9090.
(325) Rharbi, Y.; Yekta, A.; Winnik, M. A.; DeVoe, R. J.; Barrera, D. *Macromolecules* **1999**, *32*, 3241.
(326) Walters, K. A.; Ley, K. D.; Schanze, K. S. *Langmuir* **1999**, *15*, 5676.
(327) Mcquade, D. T.; Pullen, A. E.; Swager, T. M. *Chem. Rev.* **2000**, *100*, 2537.
(328) Swager, T. M. *Acc. Chem. Res.* **1998**, *31*, 201.
(329) Chen, L. X.; Jäger, W. J. H.; Gosztola, D. J.; Niemczyk, M. P.; Wasielewski, M. R. *J. Phys. Chem. B* **2000**, *104*, 1950.
(330) Wong, K. T.; Lehn, J. M.; Peng, S. M.; Lee, G. H. *Chem. Commun.* **2000**, *22*, 2259.
(331) Wolcan, E.; Ferraudi, G. *J. Phys. Chem. A* **2000**, *104*, 9281.

An extensive synthetic chemistry has evolved in this area based on the derivatization of PS by added polypyridyl complexes.[34] The polymers are prepared by free-radical or living anionic polymerization typically with 15−30 average repeat units, which can be varied by varying the polymerization conditions.

Anionic polymerization gives lower polydispersities and narrower molecular weight distributions. These polymerizations are carried out with protected, silylated amine groups, $-N(SiMe_3)_2$, to avoid reactions with the alkyllithium initiators. They are later deprotected by acid hydrolysis to give the amine. Functional groups are added by amide bond formation to modules functionalized as carboxylic acid derivatives, e.g., $PS-(CH_2)_n-NH_2 + [M(4\text{-}COOH\text{-}4'\text{-}Mebpy)(bpy)_2)]^{2+} \rightarrow PS-(CH_2)_n-NHC(O)-(4'\text{-}Mebpy)M(bpy)_2]^{2+} + H_2O$ (M = Os, Ru). The extent of loading by amide bond formation can be controlled by limiting the added reagent. Bi- and multifunctional polymers can be prepared by adding additional groups in subsequent steps.[48,94,109] The structure shown in Figure 7 illustrates the repeat units in a mixed polymer of this kind. In the example shown there, the polymer was a 1:1 mixture of styrene and derivatized styrene.

In fully loaded polymers, the excluded volume occupied by the added complexes is large given their diameters of 13−14 Å. This is considerably larger than a repeat unit of the polymer backbone, 5−6 Å. The resulting size discrepancy results in linear rodlike structures, as shown in Figure 12 for the structure of $[[PS-(CH_2)_2-C(O)NH-(Ru^{II})_{20}](PF_6)_{40}$ calculated by a Monte Carlo simulation.[94]

On the basis of this strategy, mixed Ru(II)−Os(II) polymers such as $[PS-(CH_2)_2-C(O)NH-(Ru^{II})_{17}(Os^{II})_3](PF_6)_{40}$ were prepared, in which rapid, intrastrand energy transfer occurs.[94,109] Also prepared was an "antenna−reaction center" polymer, in which antenna sensitization of local electron transfer was demonstrated [section III.B(ii) and Figure 7].[97] In the latter polymer, an additional, long-lived transient (>1 ms) appears in which $MV^{\bullet+}$ and $PTZ^{\bullet+}$ are spatially separated (eq 39). This is an important result because it points to pathways where spatially separated redox equivalents can be produced on single polymer strands, which may be useful for driving separate fuel-forming half-reactions.

$$\text{-(MV}^{2+}\text{-Ru}^{II}\text{-PTZ)-(Ru}^{II}\text{)}_n\text{-(MV}^{2+}\text{-Ru}^{II}\text{-PTZ)-} \xrightarrow{+h\nu} \text{-(MV}^{+}\text{-Ru}^{II}\text{-PTZ)-(Ru}^{II}\text{)}_n\text{-(MV}^{2+}\text{-Ru}^{II}\text{-PTZ}^{+}\text{)-} \quad (39)$$

Oligoprolines. Derivatization of preformed polymers in the manner described here is inherently random. It is possible to have control over content but not over spatial organization. A block copolymer strategy with sequential polymerization, e.g., −D−D−D−C−C−C−, may be viable but not for spatial control at the single-module level.

Solid-state peptide synthesis offers control over both.[332] In this approach, an initial amino acid is chemically attached to a solid support, typically a PS bead, with the remaining, unreacted functional group, $-NH_2$ or −COOH, chemically protected. In the sequence in eq 40 with P representing the PS bead, (1,1-dimethylethoxy)carbonyl (Boc) is used as the protecting group. Subsequent deprotection and coupling to a second protected amino acid begins the step-by-step synthesis of complex oligopeptides with spatial control. The final oligopeptide is displaced chemically from the support.

$$\begin{aligned} P-C(O)C(R)NH-Boc &\xrightarrow{-Boc} \\ P-C(R)NH_2 &\xrightarrow{+Boc-NHC(R')CO_2H} \\ P-C(O)C(R)NHC(O)C(R')NH-Boc \quad (40) \end{aligned}$$

A D−C−A assembly product of this strategy is illustrated in Figure 13. It is based on proline, the only natural cyclic amino acid. Oligoprolines tend to form stable helical structures if there are at least 6−8 contiguous prolines. This introduces an element of three-dimensional spatial control, allowing alignment of the three functional groups on a single side of the oligoproline helix, as shown in Figure 13. In this assembly, MLCT excitation of the Ru(bpy) chromophore is followed by reductive quenching by PTZ, ultimately giving the $Anq^{-}-Ru^{II}(bpy)-PTZ^{+}$ RSS with efficiencies as high as 86% depending on the solvent (section IV.E and Scheme 5).[254]

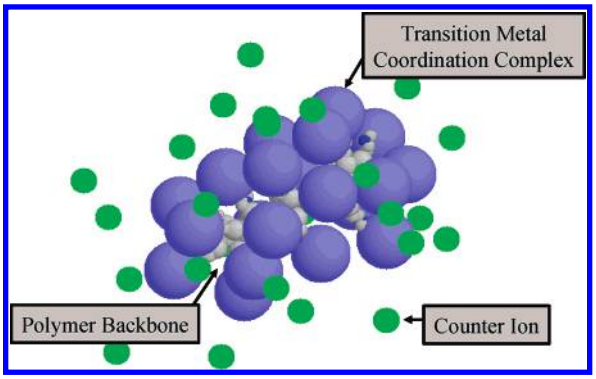

Figure 12. Molecular structure of $[PS-(CH_2)_2-C(O)NH-(Ru^{II})_{20}](PF_6)_{40}$ from a Monte Carlo simulation.[94]

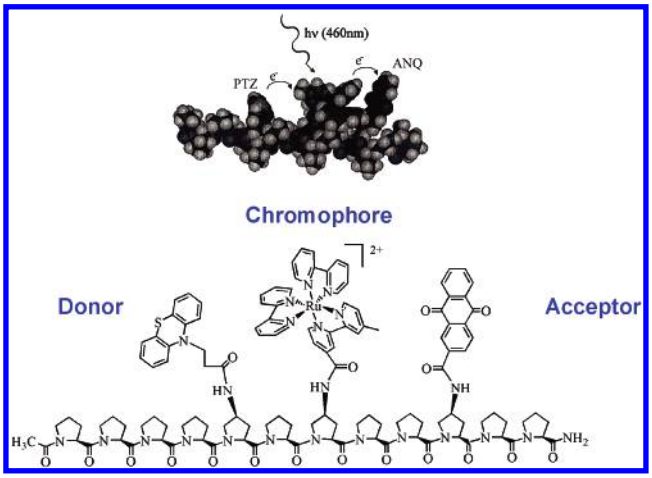

Figure 13. Oligoproline donor (PTZ)−chromophore [Ru(bpy)]−acceptor (quinone) D−C−A assembly illustrating electron transfer following MLCT excitation.

(332) Erickson, B. W.; Merrifield, R. B. *Proteins* **1976**, *2*, 255.

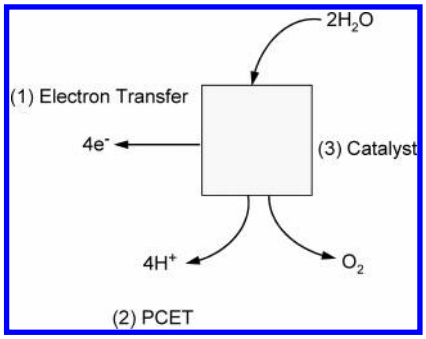

Figure 14. Essential elements for an electron-transfer-driven solar half-reaction for water oxidation showing integration of electron transfer, PCET, and catalysis.

The initial results suggest that the oligoproline strategy is viable for constructing a broad class of molecular assemblies. As noted above, this approach offers control over local spatial content and long-range three-dimensional order by exploiting the tendency toward helix formation. Control over local and long-range structures has been used to advantage in the study of solvent and distance effects in energy and electron transfer.[34,240,254,333]

VIII. Assembling the Assemblies in Device-like Configurations

A higher level hierarchy beyond molecular assemblies and an assembly-of-assemblies strategy are required for a working device. There are a number of candidates based on nanoparticle or organic films, membranes, gels or colloids, or other inert porous substrates. Multilayers are required for high light absorptivity and an interface where excitation and coupled reactions can occur with both products and reactants equilibrated with the external environment.

VIII.A. Half-Reaction Assemblies. The modular approach requires integration of energy-conversion half-reaction assemblies where oxidative or reductive catalysis occurs. In these assemblies, there are three common elements—(1) electron transfer, (2) PCET, and (3) catalysis—as illustrated for water oxidation in Figure 14.

(1) Electron Transfer. The source of electrons in Figure 14 is generic and could conceivably come from a molecular excitation/electron transfer cycle, a photovoltaic (P−V) source, or even a natural photosynthetic membrane. There is a requirement for the buildup of four redox equivalents by electron transfer in order for O_2 to be evolved.

(2) PCET, H^+ Channeling. PCET avoids the accumulation of charge resulting in redox potential leveling, access to multiple oxidation states, and catalyst activation. Coupled EPT may be required to avoid intermediates that are at high energy in proton content. There is also a requirement for proton channeling to the external environment as found in biomembranes. Proton channeling maintains a proton balance, avoiding a buildup or depletion in the local proton inventory.

(3) Catalysis. Multielectron transformations are carried out at catalysts that utilize complex pathways such as O- or H-atom transfer, hydride transfer, oxidative addition, reductive elimination, insertion, or EPT. They must occur on the approximately millisecond time scale or shorter to avoid being rate-limiting given the incident solar irradiance. Pathways can also be envisaged in which single-photon, single-electron activation leads to intermediates that are themselves photoactive, toward the release of O_2, for example.

VIII.B. Membrane Assemblies in Natural Photosynthesis. Photosystem II. Natural photosynthetic systems utilize membranes for assembling key photosynthetic modules and separating products.[24,26,40,334−336] The key elements in Figure 14 are all present in photosystem II. (1) *Electron transfer*. Water oxidation at the $CaMn_3$ cluster, the OEC, is initiated by $Y_Z \rightarrow P_{680}^* \rightarrow Q_A$ electron transfer. The OEC is subsequently activated oxidatively by OEC $\rightarrow Y_Z^\bullet$ electron transfer. (2) *PCET−EPT*. Both electrons and protons are lost by PCET in the stepwise oxidation of the OEC through the Kok cycle. A thermodynamic analysis suggests that intermediates that are at high energy in proton content at both Y_Z and the OEC are avoided by EPT. It has been proposed that electron transfer occurs from $Mn^{n+}-OH_2$- - -$^-$OOC(Asp-61) to TyrO$^\bullet$- - -$^+$H−His-190 accompanied by proton transfer at both sites by a 1 $e^-/2H^+$ MS-EPT pathway to give Mn^{n+1}−OH- - -HOOC(Asp-61) and TyrO−H- - -His-190.[264] Asp-61 lies near the OEC and is at the entryway to a proton channel to the exterior of the membrane (the lumen), which enables proton equilibration. (3) *Catalysis*. Catalysis may be localized at Mn(4) appended to the $CaMn_3$ core, with stepwise PCET leading from $Mn^{II}-OH_2$ to $Mn^V{=}O$. As shown in eq 38, the O- - -O bond-forming step may involve OH^- attack on the oxo group to give a $Mn^{III}-OOH$ intermediate.[24,264,299,300]

VIII.C. Ru(bpy) Assemblies. It is possible to envisage a number of approaches to creating hierarchial assemblies for artificial photosynthesis based on polypyridyl complexes.

(i) SiO_2-Based Sol−Gels. SiO_2-based sol−gels are formed by acid hydrolysis of alkoxysilanes, $Si(OR)_4$ (R = Me, Et). In the presence of added organic polyether molecules as stabilizers, gels form that are chemically inert and have open porous structures, which are optically transparent.[337−342] Sol−gel films incorporating redox-active components have been formed on electrode surfaces, which provide a basis for electrochemistry and long-range electron transfer both to the underlying electrode and to an external solution.[343−348]

(333) McCafferty, D. G.; Friesen, D. A.; Danielson, E.; Wall, C. G.; Saderholm, M. J.; Erickson, B. W.; Meyer, T. J. *Proc. Natl. Acad. Sci. U.S.A.* **1996**, *93*, 8200.
(334) Fenna, R. E. M. B. W. *Nature* **1975**, *258*, 573.
(335) Zouni, A.; Witt, H.-T.; Kern, J.; Fromme, P.; Krauss, N.; Saenger, W.; Orth, P. *Nature* **2001**, *409*, 739.
(336) Kamiya, N.; Shen, J.-R. *Proc. Natl. Acad. Sci. U.S.A.* **2003**, *100*, 98.
(337) In *Better Ceramics Through Chemistry II*; Brinker, C. J., Clark, B. E., Ulrich, D. R., Eds.; Materials Research Society: Pittsburgh, PA, 1986; Vol. 73.
(338) Brinker, C. *J. Non-Cryst. Solids* **1988**, *100*, 31.
(339) Brinker, C. J.; Scherer, G. W. *Sol−Gel Science: The Physics and Chemistry of Sol−Gel Processing*; Academic Press: Boston, 1990.
(340) Hench, L. L.; Ulrich, D. R. *Science of Ceramic Chemical Processing*; Wiley: New York, 1986.
(341) Hench, L. L.; West, J. K. *Chem. Rev.* **1990**, *90*, 33.
(342) Dunn, B.; Zink, J. I. *J. Mater. Chem.* **1991**, *1*, 903.
(343) Avnir, D. *Acc. Chem. Res.* **1995**, *28*, 328.
(344) Levy, D. *Chem. Mater.* **1997**, *9*, 2666.

A number of relevant observations have been made in these media: (1) Electrochemistry, electroluminescence (el), and electrochemiluminescence (ecl) have been observed in sol−gels containing the Ru^{II}-derivatized PS polymer [PS−$CH_2CH_2NHC(O)-(Ru^{II})_{18}](Cl)_{36}$ on the surface of Sn^{IV}-doped In_2O_3 (ITO) electrodes.[349,350] (2) It has been shown that facile intrastrand energy transfer continues to occur in a $Ru^{II}-Os^{II}$-derivatized PS polymer.[351,352] (3) Photo- and electrochemically active composite structures have been prepared by reductive electropolymerization of $[M(vbpy)_3]^{2+}$ (M = Ru, Os; vbpy is 4-vinyl-4-Mebpy; see below) in the open pores of SiO_2 sol−gel films on ITO. The growth of the electropolymerized polymer chains occurs through parallel diffusion channels in the sol−gel structure.[353]

(ii) Electropolymerized Thin Film Structures. Thin polymeric films of metal polypyridyl complexes containing the vinylbipyridine (vbpy) or pyrrolylbipyridine (pyr-bpy) ligands can be prepared by electropolymerization on a variety of conducting substrates. The ligand structures are shown below.[354,355] The vbpy films are prepared by reductive scans through bpy-based π^* reductions in the potential region −0.7 to −1.7 V vs SSCE in CH_3CN. Ligand-based reduction initiates polymerization at the electrode surface. For complexes such as $[Ru(vbpy)_3]^{2+}$, which contain multiple vbpy ligands, stable cross-linked network polymer films form on the electrode. Film thicknesses can be varied from a few monolayers to microns by varying the scan rate and the concentration of the complex in the external solution. A similar procedure for pyrrole-containing ligands, but with oxidative scans past +0.8 V, also results in well-defined thin films. Other vinyl- and pyrrole-containing ligands have been electropolymerized as well.

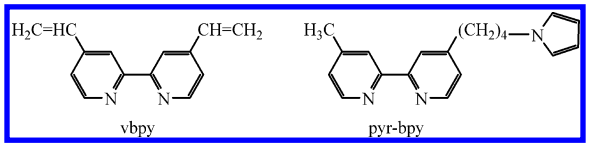

Electropolymerization has been used to create a variety of film structures, some of which could find application in assembling elements for artificial photosynthesis. They include (1) bilayers by sequential polymerization of $[Ru(vbpy)_3]^{2+}$, followed by $[Os(vbpy)_3]^{2+}$, for example, in which rectification (electron transfer in one direction) has been observed;[356] (2) pH-induced electron transfer from an outer film−solution interface across an inner film layer;[357] (3) photocurrent effects and electroluminescence;[358] (4) electropolymerized overlayer stabilization of an adsorbed chromophore on TiO_2;[359] (5) creation of molecular voids for size-selective diffusion and micron-level image formation;[235,360−367] (6) formation and reactivity of catalytically active Ru^{IV}═O and O═Ru^{VI}═O sites imbedded in film structures[368] with spatial control;[369] and (7) electropolymerization of electro- and photoactive films of PS-derivatized "macromers", containing multiple linked Ru(vbpy) complexes, and of large, preformed molecular assemblies.[370,371]

(iii) Adsorption on Oxide Surfaces. Strategies exist for facile surface binding of photo- and electroactive modules to oxide surfaces through carboxylic acid, phosphonic acid, or siloxy derivatives, with $-P(O)(OH)_2$ kinetically less labile than −COOH and stable in aqueous environments at pH < 7.

Nanoparticle thin films formed by sol−gel technology and other highly porous, high-surface-area, optically transparent oxides offer the advantages of multilayer structures for achieving high light absorptivities, ease of fabrication on surfaces, and the availability of a variety of surface oxides and oxide structures.[51,372−376]

Films of TiO_2 are electrochemically and photochemically active, ZrO_2 is inert, and doped SnO_2 is a conductor. Multimicron-thick films can be prepared on a variety of substrates including glass and ITO optically transparent electrodes.

(345) Dvorak, O.; DeArmond, K. M. *J. Phys. Chem.* **1993**, *97*, 2646.
(346) Castellano, F. N.; Heimer, T. A.; Tandhasetti, M. T.; Meyer, G. J. *Chem. Mater.* **1994**, *6*, 1041.
(347) Castellano, F. N.; Meyer, G. J. *Molecular Level Artificial Photosynthetic Materials*; John Wiley & Sons: New York, 1997; pp 167−208.
(348) Innocenzi, P.; Kozuka, H.; Yoko, T. *J. Phys. Chem. B* **1997**, *101*, 2285.
(349) Sykora, M.; Maxwell, K. A.; Meyer, T. J. *Inorg. Chem.* **1999**, *38*, 3596.
(350) Rubinstein, I.; Martin, C. R.; Bard, A. J. *Anal. Chem.* **1983**, *55*, 1580.
(351) Fleming, C. N.; Papanikolas, J. M.; Meyer, T. J., unpublished observations.
(352) Fleming, C. N.; Jang, P.; Meyer, T. J.; Papanikolas, J. M. *J. Phys. Chem. B* **2004**, *108*, 2205.
(353) Yang, J.; Sykora, M.; Meyer, T. J. *Inorg. Chem.* **2005**, *44*, 3396.
(354) Murray, R. W. *Molecular Design of Electrode Surface*; John Wiley and Sons: New York, 1992.
(355) Deronzier, A.; Moutet, J. C. *Coord. Chem. Rev.* **1996**, *147*, 339.
(356) Abruna, H. D.; Denisevich, P.; Umana, M.; Meyer, T. J.; Murray, R. W. *J. Am. Chem. Soc.* **1981**, *103*, 1.
(357) Vining, W. J.; Surridge, N. A.; Meyer, T. J. *J. Phys. Chem.* **1986**, *90*, 2281.
(358) Surridge, N. A.; McClanahan, S. F.; Hupp, J. T.; Danielson, E.; Gould, S.; Meyer, T. J. *J. Phys. Chem.* **1989**, *93*, 294.
(359) Moss, J. A.; Yang, J. C.; Stipkala, J. M.; Wen, X.; Bignozzi, C. A.; Meyer, G. J.; Meyer, T. J. *Inorg. Chem.* **2004**, *43*, 1784.
(360) Gould, S.; Meyer, T. J. *J. Am. Chem. Soc.* **1991**, *113*, 7442.
(361) MacKay, S. G.; Bakir, M.; Musselman, I. H.; Meyer, T. J.; Linton, R. W. *Anal. Chem.* **1991**, *63*, 60.
(362) Gray, K. H.; Gould, S.; Leasure, R. M.; Masselman, I. H.; Lee, J. J.; Meyer, T. J.; Linton, R. W. *J. Vac. Sci. Technol.* **1992**, *10*, 2679.
(363) Musselman, I. H.; Gray, K. H.; Leasure, R. M.; Meyer, T. J.; Linton, R. W. *Microanal.* **1993**, *2*, 297.
(364) Gould, S.; Leasure, R. M.; Meyer, T. J. *Chem. Br.* **1995**, *31*, 891.
(365) Gould, S.; Gray, K. H.; Linton, R. W.; Meyer, T. J. *J. Phys. Chem.* **1995**, *99*, 16052.
(366) Leasure, R. M.; Ou, W.; Moss, J. A.; Linton, R. W.; Meyer, T. J. *Chem. Mater.* **1996**, *8*, 264.
(367) Gould, S.; O'Toole, T. R.; Meyer, T. J. *J. Am. Chem. Soc.* **1990**, *112*, 9490.
(368) Guadalupe, A. R.; Chen, X. H.; Sullivan, B. P.; Meyer, T. J. *Inorg. Chem.* **1993**, *32*, 5502.
(369) Leasure, R. M.; Moss, J. A.; Meyer, T. J. *Inorg. Chem.* **1994**, *33*, 1247.
(370) Leasure, R. M.; Kajita, T.; Meyer, T. J. *Inorg. Chem.* **1996**, *35*, 5962.
(371) Kajita, T.; Leasure, R.; Devenney, M.; Friesen, D.; Meyer, T. J. *Inorg. Chem.* **1998**, *37*, 4782.
(372) Garcia, C. G.; deLima, J. F.; Iha, N. Y. M. *Coord. Chem. Rev.* **2000**, *196*, 219.
(373) Kalyanasundaram, K.; Grätzel, M. *Coord. Chem. Rev.* **1998**, *177*, 347.
(374) Bignozzi, C. A.; Schoonover, J. R.; Scandola, F. *Prog. Inorg. Chem.* **1997**, *44*, 1.
(375) Gerfin, T.; Grätzel, M.; Walder, L. *Prog. Inorg. Chem.* **1997**, *44*, 345.
(376) O'Regan, B.; Grätzel, M. *Nature* **1991**, *353*, 737.

Scheme 10. Schematic Diagram Illustrating a Photoelectrochemical Cell for the Dehydrogenation of 2-Propanol to Acetone and Hydrogen[a]

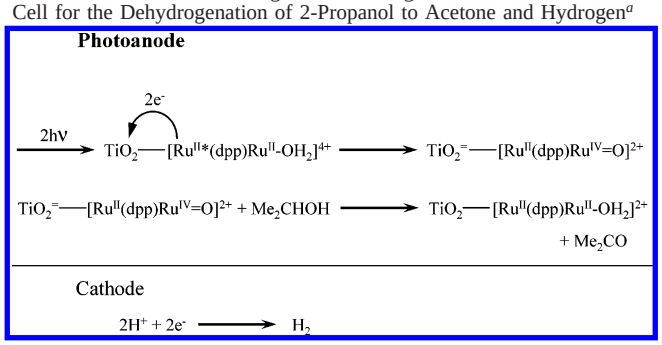

[a] The structure of the adsorbed chromophore catalyst is shown in section II.B.

A number of relevant observations have been made on these surfaces:

(1) "Antenna" energy transfer has been observed from surface-bound Ru^{II}* to Os^{II} on ZrO_2[110] as well as cross-surface electron transfer on mixed surfaces.[377]

(2) Excitation of $[Ru(4,4'\text{-}(COOH)_2bpy)(bpy-PTZ)(bpy-MV^{2+})]^{4+}$ adsorbed to ZrO_2 gives $(MV^{\bullet+})Ru(PTZ^{\bullet+})$, which subsequently undergoes $MV^+ \rightarrow PTZ^+$ back electron transfer on the same time scale ($\tau \sim 140$ ns) as in solution. A competing pathway gives spatially separated $(MV^{\bullet+})Ru(PTZ)$ and $(MV^{2+})Ru(PTZ^{\bullet+})$, and back electron transfer is far slower, >1 ms, depending on surface coverage.[378]

(3) As mentioned in section 1, dehydrogenation of 2-propanol in 2-propanol was observed upon excitation of $[(4,4'\text{-}(CO_2H)_2bpy)(4,4'\text{-}Me_2bpy)Ru_a^{II}(dpp)Ru_b^{II}(tpy)(OH_2)]^{4+}$ adsorbed to TiO_2 by the series of reactions in Scheme 10.[53]

(4) In the presence of added hydroquinone and water, excitation of $[Ru(4,4'\text{-}(PO_3H_2)_2bpy)(bpy)_2]^{2+}$ and $[Ru(tpy)(4,4'\text{-}(PO_3H_2)_2bpy)(H_2O)]^{2+}$ coadsorbed to TiO_2 results in incident photon-to-current efficiences of up to 8%. The net reaction is the dehydrogenation of hydroquinone (H_2Q) to quinone (Q)

$$H_2Q \xrightarrow{+2h\nu} Q + H_2$$

with H_2 produced at a platinized-platinum cathode.[379]

IX. Final Comments

The twin challenges of diminishing petroleum and natural gas supplies, with their implications for national energy security, and the impact of greenhouse gases on global warming make long-term energy solutions based on renewable energy sources a mandate for current and future research. This includes artificial photosynthesis with the promise of creating fuels from solar energy, a goal that will become increasingly relevant in the years to come. The horizon for definable oil reserves is shrinking, and there is the promise that hydrogen could become the transportation fuel of the future in hydrogen/oxygen fuel cells. Because hydrogen is not found uncombined to any extent in nature, its generation requires the input of energy, and the most attractive energy source is the sun, with water as the hydrogen source.

The approach to water splitting and other fuel-forming reactions described here based on molecular excited states and their reactions originated in the early 1970s[60−64,305,380−382] and continues to be of interest today.[260,383−385]

In the interim, much has been learned about energy and electron transfer and about more complex redox pathways based on atom transfer, hydride transfer, insertion, and coupled EPT. Catalysts have been created for water oxidation and CO_2 reduction. MLCT excited states are well understood, and the synthesis of d^6 polypyridyl complexes has become a cottage industry. Strategies have evolved for preparing complex molecular assemblies, and the excited- and ground-state properties of metal complexes and molecular assemblies are routinely investigated on surfaces and in rigid media on time scales as short as hundreds of femtoseconds.

The importance of artificial photosynthesis should not be overlooked. Solving the problem of harnessing solar energy to create hydrogen from water reliably and inexpensively would have a remarkably positive impact on our energy future.

Acknowledgments are made to the many former members of the Meyer research group who have contributed to this area over a period of 30 years, to long-lasting and highly productive collaborations with faculty colleagues at the University of North Carolina (Dave Whitten, Royce Murray, Rich Linton, Bruce Erickson, John Papanikolas, and Joe DeSimone), and to funding from NSF, DOE, ARO-D, the Gas Research Institute, and the LDRD program at Los Alamos National Laboratory for research support.

IC050904R

(377) Trammell, S. A.; Meyer, T. J. *J. Phys. Chem. B* **1999**, *103*, 104.
(378) Sykora, M.; Yang, J. C.; Meyer, T. J. *J. Phys. Chem. B* **2005**, *109*, 1499.
(379) Gallagher, L. A.; Serron, S. A.; Wen, X.; Hornstein, B. J.; Dattelbaum, D. M.; Schoonover, J. R.; Meyer, T. J. *Inorg. Chem.* **2005**, *44*, 2089.
(380) Meyer T. J. *Photochemical Energy Conversion*; Elsevier Science Publishing Co., Inc.: New York, 1989; p 75.
(381) Meyer, T. J. Excited-state electron transfer. *Inorganic Chemistry: Toward the 21st Century*; American Chemical Society: Washington, DC, 1983; Vol. 211, p 157.
(382) Sutin, N. *J. Photochem.* **1979**, *10*, 19.
(383) Meijer, M. D.; Van Klink, G. P. M.; Van Koten, G. *Coord. Chem. Rev.* **2002**, *230*, 141.
(384) Durr, H.; Bossmann, S. *Acc. Chem. Res.* **2001**, *34*, 905.
(385) Bouas-Laurent, H.; Castellan, A.; Desvergne, J. P.; Lapouyade, R. *Chem. Soc. Rev.* **2000**, *29*, 43.